Aalto University
School of Science
Master's Programme in ICT Innovation - EIT Digital Master School

Shamsul Arefeen Al Mahmud

Wireless Power Transfer:

Machine Learning Assisted Characteristics Prediction for Effective Wireless Power Transfer Systems

Master's Thesis
Espoo, September 24, 2020

September 24, 2020

Supervisors: Professor Hans-Peter Nee, KTH Royal Institute of Technology
Professor Quan Zhou, Aalto University
Advisor: Dr. Prasad Jayathurathnage, Aalto University
Evangelos Liakos, KTH Royal Institute of Technology

Aalto University
School of Science
Master's Programme in ICT Innovation - EIT Digital Master School

ABSTRACT OF MASTER'S THESIS

Author: Shamsul Arefeen Al Mahmud

Title:
Wireless Power Transfer: Machine Learning Assisted Characteristics Prediction for Effective Wireless Power Transfer Systems

Date: September 24, 2020 **Pages:** 63

Major: Electrical Engineering **Code:** ELEC3055

Supervisors: Professor Hans-Peter Nee, KTH Royal Institute of Technology
Professor Quan Zhou, Aalto University

Advisor: Dr. Prasad Jayathurathnage, Aalto University
Evangelos Liakos, KTH Royal Institute of Technology

One of the main challenges in wireless power transfer (WPT) devices is performance degradation when the receiver's position and characteristics vary. The variations in the system parameters such as load impedance and coupling strength in WPT devices affect performance characteristics such as output voltage and power. When the system parameters are different from the optimal operating conditions, the performances are degraded. Therefore, the load impedance and coupling strength must be monitored to do the necessary optimization and control. However, such control approaches require additional sensing circuits and a data communication link between transmitter- and receiver-sides. This study proposes a new machine learning assisted WPT system that predicts the power delivered to the receiver by only using measurements at the transmitter-side. In addition, a method is also proposed to estimate load impedance and coupling coefficient using machine learning approach. We study what parameters measurable at the transmitter-side can be used to predict the output power delivered to receivers at variable load impedance and coupling strengths. In the proposed method, the output power of an inductor-capacitor-capacitor (LCC)-Series tuned WPT system is successfully predicted only using the measured root-mean-square of the input current. Random forest algorithm has shown best accuracy to estimate the output power based on transmitter-side parameters only. The proposed approach is experimentally validated using a laboratory prototype. Harmonic components of the input current are used to assess the load impedance and coupling coefficient successfully. Multi-output regression has the highest accuracy for estimating the load impedance and coupling coefficient. The proposed machine learning algorithm is also used to classify the turn-on and -off regimes to ensure high-efficient operation.

Keywords: Wireless power transfer, Machine learning, Coupling strength estimation, Load impedance estimation, Multi-transmitter wireless power transfer systems

Language: English

Wireless Power Transfer

Machine Learning Assisted Characteristics Prediction for Effective Wireless Power Transfer Systems

SHAMSUL AREFEEN AL MAHMUD

Date: August 31, 2020
Supervisor: Evangelos Liakos
Examiner: Prof. Hans-Peter Nee
Advisor: Dr. Prasad Jayathurathnage
School of Electrical Engineering and Computer Science
Host organization: Aalto University
Swedish title: Trådlös kraftöverföring
Swedish subtitle: Maskininlärning Assisterade egenskaper
Förståelse för effektiva trådlösa kraftöverföringssystem

Wireless Power Transfer / Trådlös kraftöverföring

Abstract

One of the main challenges in wireless power transfer (WPT) devices is performance degradation when the receiver's position and characteristics vary. The variations in the system parameters such as load impedance and coupling strength in WPT devices affect performance characteristics such as output voltage and power. When the system parameters are different from the optimal operating conditions, the performances are degraded. Therefore, the load impedance and coupling strength must be monitored to do the necessary optimization and control. However, such control approaches require additional sensing circuits and a data communication link between transmitter- and receiver-sides. This study proposes a new machine learning (ML) assisted WPT system that predicts the power delivered to the receiver by only using measurements at the transmitter-side. In addition, a method is also proposed to estimate load impedance and coupling coefficient using machine learning approach. We study what parameters measurable at the transmitter-side can be used to predict the output power delivered to receivers at variable load impedance and coupling strengths. In the proposed method, the output power of an inductor-capacitor-capacitor (LCC)-Series tuned WPT system is successfully predicted only using the measured root-mean-square (RMS) of the input current. Random forest algorithm has shown best accuracy to estimate the output power based on transmitter-side parameters only. The proposed approach is experimentally validated using a laboratory prototype. Harmonic components of the input current are used to assess the load impedance and coupling coefficient successfully. Multi-output regression has the highest accuracy for estimating the load impedance and coupling coefficient. The proposed ML algorithm is also used to classify the turn-on and -off regimes to ensure high-efficient operation.

Keywords

Wireless power transfer, Machine learning, Coupling strength estimation, Load impedance estimation, Multi-transmitter wireless power transfer systems

Sammanfattning

En av de viktigaste utmaningarna med trådlösa kraftöverföring enheter är degraderingen av prestandan när mottagarens position och egenskaper varierar. Variationerna av systemets parametrar, såsom belastningsmotstånd och kopplings styrka i WPT-anordning, påverkar prestanda egenskaperna såsom spänning och effekt. När system parametrarna skiljer sig från de optimala drifts förhållandena, försämras prestandan. Därför måste luftmotståndet och kopplings styrkan övervakas, för att göra nödvändig optimering och kontroll. Sådana styrmetoder kräver emellertid ytterligare avkännings kretsar, och en data kommunikationslänk mellan sändar- och mottagarsidan. Denna studie föreslår ett nytt maskininlärning assisterat WPT-system, som förutsäger kraften som levereras till mottagaren genom att endast använda mätningar på sändarsidan. Dessutom föreslås en metod för att detektera belastningsimpedans och kopplings koefficient med användning av maskin inlärningsmetoder. Vi studerar vilka parametrar som är mätbara på sändarsidan och som kan användas för att förutsäga utgången effekten som levereras till mottagare vid varierande belastningsmotstånd och kopplings nivåer. I den föreslagna metoden förutses framgångs effekten för ett induktor-kondensator-kondensator LCC-serie avstämt WPT-system endast framgångsrikt med hjälp av det uppmätta effektivvärdet för ingångs strömmen. Slumpmässig skogsalgoritm har visat exceptionell noggrannhet för att uppskatta uteffekten endast baserat på sändarsidans parametrar. Den föreslagna metoden valideras experimentellt med användning av en laboratorium prototyp. Harmoniska komponenter i ingångs strömmen används för att framgångsrikt bedöma last motståndet och kopplings koefficienten. Multi-utgångsregression har verkat vara mycket exakt för att uppskatta belastningsimpedans och kopplingskoefficient. Den föreslagna maskininlärning algoritmen används också för att klassificera start-och-off-regimer för att säkerställa hög effektiv drift.

Nyckelord

Trådlös kraftöverföring, maskininlärning, uppskattning av kopplingsstyrka, uppskattning av belastningsimpedans, Multisändare trådlösa kraftöverföringssystem

Acknowledgments

The present work was carried out at the Department of Electronics and Nano-engineering of Aalto University, School of Electrical Engineering. I would like to thank Prof. Sergei Tretyakov for his diligent support, motivation and suggestions during my tenure as a student. It was an honor for me to be part of your group and contribute to its research work.

Furthermore, I would like to give a special thanks to my advisor, Dr. Prasad Jayathurathnage, for mentoring me to complete my thesis. I appreciate the invaluable support that you provided me during the thesis work. I will always be grateful for the knowledge you have shared with me.

My appreciation to my examiner, Prof. Hans-Peter Nee, for allowing me to explore the domain of wireless power transfer. I would like to thank my supervisor, Evangelous Liakos, for the support and advice he provided me throughout the master's thesis.

I would like to thank my parents and friends for their countless effort and continuous encouragement throughout my academic career. Finally, I appreciate the opportunity given by KTH Royal Institute of Technology and European Innovation and Technology (EIT) master's program.

Espoo, August 2020
Shamsul Arefeen Al Mahmud

Contents

List of Figures

List of Tables

List of acronyms and abbreviations

CAGR compound annual growth rate

DT decision tree

EMF electromotive force

EV electric vehicle

LCC inductor-capacitor-capacitor

ML machine learning

RF random forest

RMS root-mean-square

Rx receiver

SVR support vector regressor

Tx transmitter

WPT wireless power transfer

Chapter 1

Introduction

Wireless power transfer (WPT) corresponds to electrical energy transfer from an energy source to an electronic system without the use of continuous wire conductors. The transfer of electrical power to different electronic devices has developed since the introduction of electrical techniques in the 18th century. In the 19th century when Maxwell's equations were developed, radio wave phenomenon was demonstrated and the WPT concept was introduced. Nikola Tesla at the end of the 19th century [4] examined the principle of WPT. While the experiment of Tesla had not been successful, Tesla's idea has become a possibility with the advent of semiconductor technology. Because of its simplicity, WPT technology can be used in many applications. This technology has a potential to change the way of life and create a whole new range of electronic equipment. Several forms of WPT technology such as laser transfer, photoelectric transmission, radio, microwave transmission, capacitive and inductive coupling have been developed. Inductive coupling techniques based on the theory of resonance have received increased attention because they provide power with acceptable efficiency that is useful for a wide array of applications. Researchers also concentrate on the complexities of architecture of wireless power transfer devices focused on the resonance inductive coupling technique.

A typical WPT setup comprises of a transmitter (Tx) coil connected to a high-frequency (HF) source and a receiver (Rx) coil connected to the electrical load. The electromagnetic field is generated and combined with the Rx, which induces voltage in the Rx side, when HF current passes through the Tx. A major gap should be rendered between Tx and Rx in a practical application, contributing to a loosely coupled condition. By means of a magnetic coupling between transmitting and receiving coils, the WPT technique can distribute

electrical energy from the source to the load without any electrical wire [5, 6]. During the power transfer, when Rx is put in a fixed spot, this scheme is known as stationary WPT which is the conventional case of many WPT systems. Recently, WPT systems have evolved into a number of multi-Tx and multi-Rx schemes with a single Tx and a main Rx [7, 8, 9]. A dynamic WPT which seeks to wirelessly control a moving receptor (Rx) is a groundbreaking extension of WPT stationary systems. A broad variety of devices where conventional WPT can be applied, such as biomedical implants [10, 11], electrical vehicles [12], consumer [13, 14] and electronic devices [15]. On the other side, dynamic WPT's successful application covers hybrid vehicles [16, 17].
The key performance indicators for WPT systems include the device level output, power transfer efficiency (PTE), and transmitted power (TP), as well as systems level criteria such as the transmission lengths and tolerance to load impedance variations. PTE refers to WPT energy transfer efficiency, while TP refers to normalized output power to the load. Obviously, high PTE is always desirable, while high TP provides higher loading power. For WPT systems optimisation, it is therefore necessary to understand both PTE and TP. Electromagnetic coupling between each Tx and Rx is the determinant for higher efficiency as the strong coupling between Tx-Rx allows us to transfer more power than when the coupling is weak. There are several approaches to determine the optimal excitation of Txs depending on Tx-Rx mutual coupling. The main aim of this degree project is to find and investigate possibilities to sense the output power required by the load along with finding a mechanism to estimate the load impedance and coupling strength for higher power transfer efficiency.

1.1 Problem

Estimating the exact value of mutual inductance between the Tx-Rx pair along with the load impedance is necessary to evaluate the power demand of the load. Doing this on the basis of transmitter-side measurements is still an unsolved problem. It is important to understand the power requirements by the load to be able to provide power efficiently. In recent research work such as in [18], a simple technique is proposed to determine the optimal current distribution in Tx coils by estimating the mutual inductance ratios between Tx-Rx pairs using only Tx-side measurements. However, the method proposed in [18] can determine only the optimal current ratios between each Tx coil, which is not sufficient to calculate the required optimal current in the coils. For this purpose, one should know the load impedance and the exact values of

mutual inductance to evaluate the power requirement of the Rx load. Load impedance can vary depending on the power demand of each receiver; for example, charging a laptop may need more power than charging a mobile phone. Therefore, estimation of mutual inductance and load impedance using only transmitter-side measurements is a crucial part of WPT research. There is another concern about how to determine activation/deactivation of the Tx coils to enable effective and efficient power transfer to the receivers. The system complexity increases with the increase in the number of Txs; therefore, analytical approaches become extremely challenging in such multi-Tx scenarios.

1.2 Purpose

Wireless power transfer systems gaining much popularity in academia and industry nowadays define a broad research field. Such systems require evaluation and control of numerous features such as safety of the consumer, dynamic positioning of the receiver, and flexible power transmission. Since wireless charging is becoming widespread among both consumers and industries, the technology is continuously improving and becoming more common in industries all across the board. Researchers are continuously trying to develop new ways to improve the efficiency of WPT systems. Reducing the cost and complexity of the WPT system is also a great concern of research in this field. The usage of wireless technology for day-to-day and industrial use has significant possible environmental benefits. Such "modern" source of electricity would eliminate the usage of batteries, one of the most harmful contributors to landfill sites. From the ethical point of view, with respect to the energy efficiency, minimizing excessive electricity usage and reducing energy use in general encourages wireless power to become an environmentally sustainable tool that could be applied on a large scale. For instance, the practical application of near-field wireless technology on a wide scale is utilized for charging electric and hybrid vehicles and buses. Instead of making a cable connection to cars, as is actually the case, wireless infrastructures will be built into parking lots and bus stations, enabling charging to take place immediately even without the physical work of plugging in. Such applications made WPT research even more interesting and attracting. In practical applications the efficiency of the systems needs to be sufficient enough, and free positioning of the receiver is also a big concern. This work is mostly focused on highly efficient WPT systems and identifies a way to allow free positioning of the receiver.

1.3 Goals

Electromagnetic coupling between each Tx and Rx is the determinant for efficiency as strong coupling between Tx-Rx allows us to transfer more power than when the coupling is weak. There are several approaches to determine the optimal excitation of Txs, depending on Tx-Rx mutual coupling. For example, in [18] optimal current distribution in the Tx side is determined by estimating the mutual inductance between Tx-Rx pairs. Similarly, in [19], coil current in each Tx is optimized depending on the mutual coupling between each Tx and Rx. However, such designs require measurements from both Tx- and Rx-sides, data communication channels, and complex control circuits, which will, in turn, increase the cost of the WPT devices. On the other hand, in [20], a novel WPT system is considered for drone applications where machine learning algorithms are applied to predict the receiver position. It is expected that the use of proper machine learning techniques can help us to solve the problem of finding optimal current distributions in transmitters without the need of measurements at the receiver side and complicated and costly communication circuits.
The main goal of this thesis project is to develop a simple and efficient approach to excite multi-Tx WPT systems without any sensors from the Rx-side by accurate estimations of the mutual inductance between the Tx-Rx pair along with the load impedance, which is necessary to evaluate the power demand of the load. The second research direction is to study the possibilities of applying ML techniques to develop a better decision-making process for optimal excitation of multiple Tx-Rx WPT systems.

1.4 Research methodology

The research methodology is determined by the goals of this project, which is focused on identifying an effective way to estimate the power requirements by the Rx load and deliver power according to the demand. Additionally, estimating load impedance and coupling coefficient to ensure free positioning of the receiver. The secondary scope of this research work is to develop a better decision-making process for optimal excitation of multiple Tx-Rx systems. The primary task is to gather knowledge by studying the state of the art. Parallel to the theoretical study, developing and simulating circuits is given priority, in order to generate practical data for the research. Analytical modeling needs to be done to identify the important factors that are closely related

to measure mutual inductance and load impedance. Recent publications and articles related to this field are used to gather knowledge about recent trends and methods. The thesis work extends the initial study presented in paper [18]. In addition to the system characteristics at the fundamental harmonic frequency, the system characteristics at higher-order harmonics are analyzed to develop a theoretical model of power demand estimation. LTSpice and eagle software are used to design power converters, simulate the circuits and design PCB layout. After developing the circuit, practical experiments are done to verify the proposed approach. A study on high-frequency inverters for a wide operating range (i.e. a wide range of coupling coefficient and load impedance) is also conducted. Next, the proposed approach is extended to multi-Tx WPT systems, with the use of the ML method to identify and differentiate multiple load impedance.

1.5 Contribution

The primary contributions of the thesis are detailed below:

- *Machine learning assisted estimation of output power using transmitter side measurement only* – Estimation of the output power using measurements only at the transmitter side is studied in this thesis. In recent studies, many researchers proposed to use feedback control from sensors at the receiver side to estimate the power level of the load. In contrast, in this work, only transmitter side measurement is used without utilization of any sensors or feedback from the receiver. A machine learning approach is introduced in this work to analyse the transmitter-side parameters and estimate the output power of the WPT system.

- *Estimation of load impedance and coupling coefficient* – In this work, a machine learning aided estimation of the load impedance and coupling coefficient is studied. Parallel to the theoretical study, appropriate circuits are designed and simulated in order to generate practical data for the research. Analytical modeling is carried out to identify important factors that are closely related to measurements of the coupling coefficient and load impedance.

1.6 Structure of the thesis

The thesis is organized into five chapters. In Chapter 1, the considered WPT systems are introduced. The problem statement, goals of the thesis, methodology, and the contribution of the thesis are also discussed in this chapter. Chapter 2 discusses the operating principle of WPT systems, provides a literature review of WPT systems, machine learning in WPT research and discusses market growth of WPT.
In Chapter 3, research paradigm is discussed, for both single and multi-transmitter systems. In this chapter, system analysis is presented through equivalent circuit analysis by explaining all the circuit equations. Chapter 4 presents the main results, where analytical, simulation, and experimental results are discussed both for estimation of the output power and estimation of the load impedance and coupling coefficient. Finally, in Chapter 5, the thesis outcomes are summarized and limitations are mentioned. Also, the future scope of research in the field of this thesis is discussed in this chapter.

Chapter 2

Background

2.1 Operating principle of WPT

Wireless charging or inductive charging is based on Faraday's law of induction [21], which states that a changing magnetic flux will cause electromotive force (EMF) in the coil. EMF is not a force, but rather a potential measured in volts between the coil's open ends. This potential generates an electrical field that controls the current on a circuit attached to the EMF source.

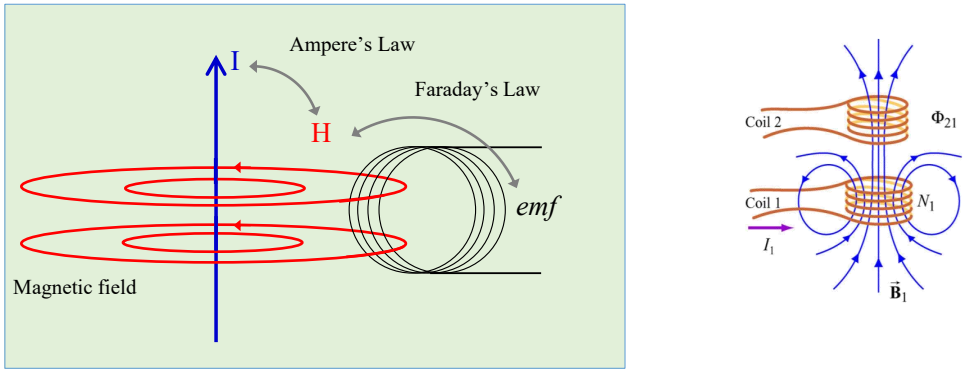

Figure 2.1 – Baisc principle of WPT. (a) the operating laws behind WPT systems, and (b) inductively coupled two coils.

As illustrated in Figure 2.1a, when there is a time-varying current in a conductor, it generates time-varying magnetic field around it according to Ampere's law [22]. Then, according to Faraday's law, when we bring another coil coupled with the time-varying magnetic field, it will induce an EMF. This EMF

can be used to power an electrical load. This is the basis of any inductive WPT system. Figure 2.1b shows two coils that are electromagnetically coupled, where there is an ac current I_1 is flowing in coil 1 that creates magnetic field $\vec{B_i}$. Magnetic flux ϕ_{21} passes through coil 2 due to the field created by coil 1. The induced EMF ϵ in coil 2 can be obtained as

$$\epsilon = -\frac{d\phi_{21}}{dt} = -\frac{d}{dt}\iint_{\text{coil2}} \vec{B_1} \cdot d\vec{A_2}$$

The rate of change of magnetic flux ϕ_{21} is proportional to the rate of change in the current in coil 1. The physical quantity mutual inductance M is defined as the proportionality constant.

$$\frac{d\phi_{21}}{dt} = M\frac{dI_1}{dt}$$

Mutual inductance M can be obtained as,

$$M = \frac{\phi_{21}}{I_1} = \frac{\iint_{\text{coil2}} \vec{B_1} \cdot d\vec{A_2}}{I_1}$$

The coupling coefficient k is defined as,

$$k = \frac{M}{\sqrt{L_{\text{tx}} L_{\text{rx}}}}$$

where L_{tx} and L_{rx} are inductance of the Tx and Rx coils, respectively. In the following section, different applications of WPT are mentioned and the application of this work has been discussed.

2.2 Applications of WPT

WPT could replace the conventional charging schemes in use today. Rather than plugging in a mobile phone or a laptop using a power cord to charge the device, wireless electricity can be harnessed and mounted in the home so that a laptop and phone operate constantly and wirelessly without the need to plug them in. Higher-level uses include charging of electric vehicle (EV). Now that EVs are more and more common on the roads, the viability of driving such a car can be maximized by stationary and even mobile WPT systems. WPT has recently been widely used in household appliances, robotics, portable electronics, underwater equipment, implantable medical devices, and electric vehicle charging [23, 24, 25, 14, 26] due to its convenience, flexibility, relia-

bility and safety. Other applications of WPT include

- Powering moving objects, such as fuel-free airplanes and drones, fuel-free rockets and running robots;
- Powering integrated circuits, consumer electronics such as mobile phones, smart watch etc.
- Powering wireless sensors.

A WPT system can be configured for common electronic devices in daily life, such as mobile phones, smart watches, laptops and many more things. The proposed method in this thesis work will allow users to place their devices anywhere within the transmitting zone. Then the system will automatically detect and turn on the nearby transmitters to charge the device efficiently. Rest of the transmitter will be turned off so that there will be no unwanted exposure to the users.

2.3 Machine learning in WPT

Machine learning algorithms employ statistics to identify trends in an enormous volume of data [27]. And the data, here, contains a lot of things — numbers, phrases, photos, clicks, many more things. If it can be stored digitally, then it can be fed into a machine-learning algorithm. Machine learning is a mechanism that empowers all of the tools we use today — recommendation platforms like Hulu, YouTube, and Spotify; search engines like Google and Baidu; social media networks like Facebook and Twitter; digital assistants like Siri and Alexa.
As illustrated in Figure 2.2, there are few steps to build a machine learning model. The first pillar of machine learning is the data. Data can be collected from many sources such as openly available data repositories, or generating data from simulation or hardware. Then the raw data is fed into data processing tools to create a structured data that can be applied to machine learning models. The processed data is run through different machine learning algorithms and try to match their error percentage or accuracy. Based on the accuracy, a model is selected and then deployed in the desired application. Most important steps of creating a machine learning model for this thesis project are discussed in brief in this section.

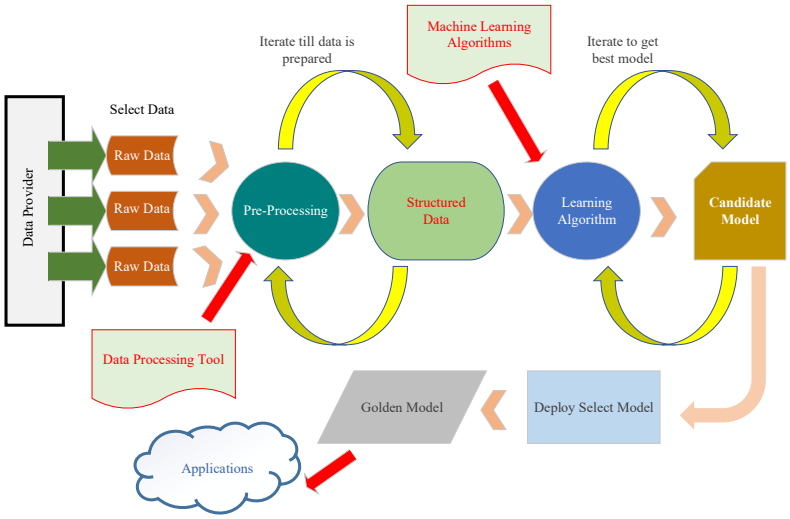

Figure 2.2 – Process of machine learning model building that illustrates different functional blocks of machine learning including, pre-processing, structuring data, algorithm selections.

2.3.1 Data collection

Data generation is the process of creating a database that will be used for different machine learning algorithms. Data can be collected in different forms. For this particular research work, LTspice simulation, Matlab code based and experimental data generation techniques are considered. A wireless power transfer system shown in Figure 3.2, based on a single transmitter and single receiver WPT circuit is developed and simulated in LTspice.

2.3.2 Feature extraction

The data set is investigated to understand the relation between different parameters (features) which could allow us to identify the power delivered to the receiver. The output power is considered as the target, while the other parameters are considered as features.

2.3.3 Data cleaning

Data cleaning is the process of cleaning and standardizing the data to make it error-free for the analysis. This process consists of various steps such as removing rows with empty values, correcting the date format, standardizing the data, and removing the outliers [28].

2.3.4 Feature engineering

Feature engineering is the process of using domain knowledge to remove unwanted features that add no value, and creating new features from the existing ones. Feature engineering is very important also to ensure that the input data is fully compatible with the algorithm. In this case we removed such features as the names of the normalized Fourier components, the normalized phase, power efficiency, etc., that essentially hold no or negligible predictive value in this case. Categorical variables like "turn on" and "turn off" are encoded using *one hot* encoding algorithm to make them interpretable by machine learning algorithms [29]. Feature scaling of all the numerical variables was done and their values were scaled down to values between 0 and 1. Clean features are fed into a general random forest regressor to identify important features among the feature set.

2.3.5 Algorithm selection

The machine learning algorithms that were used for model building in this study are decision tree (DT), random forest (RF), and support vector regressor (SVR). These methods are selected by looking at two parameters. The first reason is that all the three algorithms are highly interpret-able which is necessary to identify the most important parameters contributing to predict the output power according to the algorithms. Though SVR may not be easily interpret-able but for a small data set SVR tends to provide nice accuracy. The second reason is that all the selected algorithms perform well even if the training data set is not huge.

Decision tree regression

Decision tree is a supervised learning method that can be applied to classification or regression problems [30]. Decision Tree approach can predict target values by learning some decision rules from the training features. Decision-tree regression uses mean squared error or mean squared deviation to measure the quality of the estimator.

Support vector regression

Support vector machine is a well-known method for solving classification problems, but it is capable of solving regression problems as well. SVR defines the acceptable level of error in the model and finds an appropriate predicted

line to fit the data [31]. Comparing to linear regression, SVR uses L2-norm of the coefficient vector to minimize the coefficients while linear regression only considers the squared error. In SVR, the absolute error is set as smaller than or equal to a specific limit, and this limit is adjusted to achieve high accuracy.

Random forest

Random forest is an ensemble technique that uses multiple decision trees to solve regression or classification problems. Random forest approach is based on bootstrap aggregation known as bagging method that trains each decision tree on a different data sample taken from the train set and predicts multiple or single output according to the need [32]. The primary idea of random forest is to combine multiple decision trees to determine the final outcome.

Hyper-parameter tuning

Hyper-parameter tuning is a process of finding the most optimal hyper-parameters for the machine learning model with the goal to increase the predictive power of the model and reduce the prediction error. In this study, algorithms like RandomSearchCV and GridSearchCV [33] were used to find the most optimal hyper-parameters for the machine learning models.

Multi-output regression

Multi output regression [34] are used to solve regression problem where two or more output prediction is required. Multiple output regressor's are available such as random forest, decision tree etc. Most learning algorithms are intended to predict a single numerical value, called regression only. Several algorithms embrace implicit multi-output regression like linear regression, decision-making trees. There are also specific models for working in which algorithms which do not help forecasting several outcomes can be bundled and exploited. The outputs usually depend on the input and each other in multi-output regression. This implies that outputs are also not independent of each other and can involve a model that forecasts all outputs together or each output depends on the other outputs. A forecast of multi-stage time series can be seen as a multi-stage regression in which the sequence of future values can be predicted and each predicted value depends on the prior sequence values.

2.4 Related work

For the last three decades, wireless charging systems have been explored for different levels of power and range of air gaps. Usually, transmitter is placed on the charging platform or a charging table, and a receiver mounted on the undercarriage of the vehicle or electric device. As the air distance between transmitter and receiver increases, or their orientation is misaligned, the coupling strength between the two coils decreases dramatically. Under this weak and changing coupling strength, the resonance characteristics and the overall efficiency of the device is changed [35]. Compensation is required to suppress inductive reactions in order to increase system performance. If the input is a voltage source, a series compensation on the transmitting side is required and the receiver side condenser may be attached in parallel or in series to the receiver coil [36]. As a consequence, the voltage-fed WPT system can be divided into series-parallel and series-types [37].
One problem for WPT implementations is the complex dynamics induced by load impedance fluctuations and mutual inductance fluctuations. The WPT system can transfer power to different devices, and the load impedance values of these devices are different. Also for charging the same unit, its equivalent load resistance changes significantly as the battery charging cycle moves from constant-current to constant-voltage mode [38]. In order to provide consumers with more ease, the receiver should be positioned with spatial independence, which ensures that the relative position of the transmitter and the receiver varies, resulting to differences in inductance. In the case of a complex wireless charging of electric vehicles, a vehicle driving on the road may be wirelessly powered; in this case, the mutual inductance of each other varies. Such unavoidable differences in load and mutual inductance would incur power fluctuations, making the WPT device deviate from its ideal operating state. Monitoring load impedance and mutual inductance is therefore important for regulating and optimizing the WPT devices.
Many methods to determining the mutual inductance and load impedance have been proposed in the literature. One approach is to use an external sensing device to sense the presence of Rx, such as a proximity sensor, which would increase costs and complexities due to the need for multiple sensing circuits [39]. Several mutual inductance calculation methods have been introduced for the use of voltage and current calculations on both Tx and Rx sides [40, 41], and for the implementation of additional detector coils on both Tx and Rx sides [39]. However, recent studies [42, 43, 44] show that load impedance and/or mutual inductance in a WPT system can be measured by

calculating input current and input voltage, eliminating receiver side sensors and contact module; thus, it can greatly simplify the circuit, minimize costs and increase efficiency. However, paper [42] deduced the differential equation of the transmitting side current; a load impedance estimating approach was suggested by examining the variance rate of the average positive envelope of this current under various loading conditions. Nevertheless, the effective range was small and the accuracy of [42] decreased when the load impedance was less than $100\ \Omega$. By the root locus system, the entire detection area was divided into two sub-regions; mathematical transient process equations were developed in each sub-region, and [43] a load impedance recognition model was introduced to expand the detection range. Nevertheless, the strategies for estimating load impedance in [42, 43] did not find differences in mutual inductance.

In recent research work such as in [18], a simple technique is proposed to determine the optimal current distribution in multiple Tx coils by estimating the mutual inductance ratios between Tx-Rx pairs using only Tx-side measurements. However, the method proposed in [18] can determine only the optimal current ratios between each Tx coil, which is not sufficient to calculate the required optimal current in the coils. For this purpose, one should know the load impedance and the mutual inductance to evaluate the power requirement of the Rx load. Therefore, estimation of mutual inductance and load impedance using only transmitter-side measurements is still remaining as an unsolved research problem. In addition, in [18], only multiple transmitters and single receiver scenarios are considered though it is possible to have multiple receivers at the same time. Then a question will arise about how to determine the current distribution of Tx coils to enable effective and efficient power transfer to all the receivers. Similarly, in [19], coil current in each Tx is optimized depending on the mutual coupling between each Tx and Rx. However, such designs require measurements from both Tx- and Rx-sides, data communication channels, and complex control circuitry's, which will in turn, increase the cost of the WPT devices. Moreover, in [20], a novel WPT system is considered for drone applications where machine learning algorithms are applied to predict the receiver position. However, the method proposed in [20] focused on identifying only the receiver position, whereas the proposed method of this thesis enables estimating the receiver position along with optimal excitation to ensure high efficient operation. This thesis project proposes to develop a simple and efficient approach to excite multi-Tx WPT systems without any sensors from the Rx-side. The system complexity increases with the increase in the number of Tx; therefore, analytical approaches

become extremely challenging in such multi-Tx scenarios.
This thesis work explores output power, load impedance and mutual inductance estimation in LCC-series compensated WPT system. The proposed methods in this thesis are completely different from previous studies. The purpose of this study is to find and investigate the possibilities to sense the power demand required by the load without using any sensors in the Rx side or any feedback network. Additionally, we will be studying possibilities of applying machine learning techniques to develop a better decision-making process for optimal excitation of multiple Tx-Rx systems.

2.5 WPT market growth

The worldwide wireless charging market encompasses very divers applications including electric vehicle charging, E-scooter charging, and consumer electronics, and robotics. The inductive WPT method is leading in the wireless charging industry and is expected to continue the same pattern in the future. The global wireless charging industry has been measured by $6514,2 millions of dollars for 2018 and is projected in $49.304,1 million by 2027 and rises by compound annual growth rate (CAGR) from 23.4 percent between 2020 and 2027, according to a recent study [45]. WPT is gaining more popularity in E-scooter, electric vehicle and automated guided vehicle sectors. The automated guided vehicle market is expected to grow to USD 2.9 billion by 2024 at a CAGR of 7.8% [46]. The e-scooter global market CAGR will have an increase of 6% in 2024 which will create a market of USD 22 billion [46]. Companies like VOI technologies are expanding the e-scooter market rapidly. The future of e-wheelchair is also promising as [47] report forecasted that global wheelchair market will be around USD 7.5 billion in 2024. These industries are looking for wireless charging solution that can enable their clients to get the freedom of positioning, safety and high efficiency. This research work is directly contributing to the current challenges that are faced by the researchers in this field and industries.

Chapter 3

System analysis

3.1 Single-transmitter WPT systems

A typical WPT system contains a high-frequency generator, transmitting coils, receiving coils, reactive compensation networks, and power receiving load, as illustrated in Figure 3.1. The utility power (either DC supply from a battery or AC mains) is converted to high-frequency using a power conversion stage, for example using a full-bridge inverter. The generator output is fed into a compensation network followed by the Tx coil. The Tx coil generates an electromagnetic field with will induce an voltage across the coupled Rx coil. The receiver circuit also encompasses a compensation circuit and a power conversion stage connected to the electrical load.

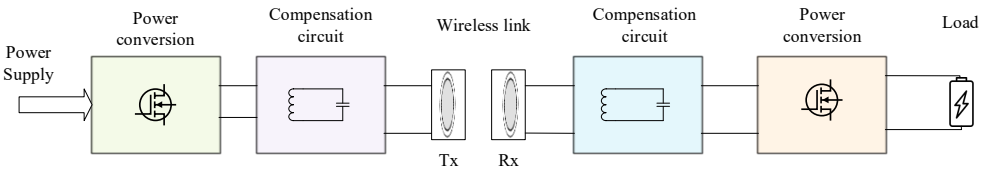

Figure 3.1 – Block diagram of a typical WPT systems

Different compensation networks has been proposed at Tx and Rx sides to improve the power transfer capability such as Series (S), Parallel (P), or, higher order compensation networks [26]. Out of these, compensation typology with LCC compensation at the Tx side and series compensation at the Rx side (LCC-S topology) exhibits load independent current source characteristics, therefore, selected for this study.

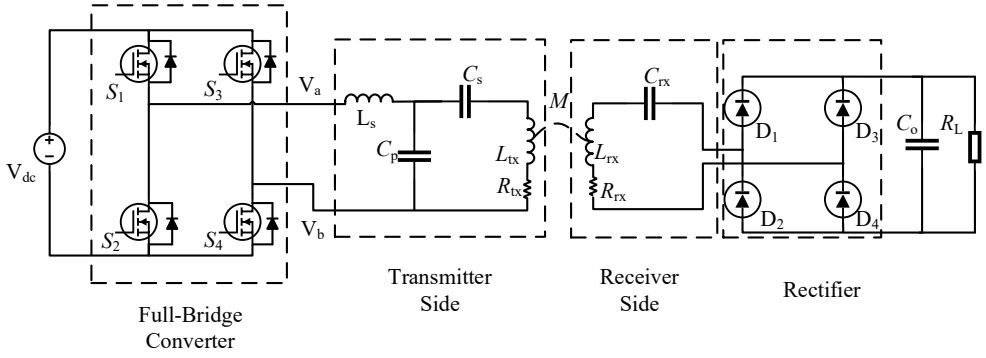

Figure 3.2 – Schematic diagram of an LCC-seris tuned WPT systems powered by a full-bridge converter.

3.1.1 The equivalent circuit analysis

Figure 3.2 illustrates the equivalent circuit diagram of LCC-S WPT circuit driven by a full-bridge converter. The LCC compensation circuit consists of a series inductance (L_s), parallel capacitor (C_p), Tx side series capacitor (C_tx), Tx coil (L_tx), receiver coil (R_rx), Rx side series capacitor (C_rx), filter capacitor (C_0) and load impedance (R_L). Internal resistances of Tx and Rx coils are R_tx and R_rx respectively. V_in is the supply voltage of the system. S_1, S_2, S_3 and S_4 are the MOSFET switches of the inverter. D_1, D_2, D_3 and D_4 are the rectifier diodes in the receiver side. The output of the full-bridge inverter produces a pulse voltage variation, and the operation of the inverter is described here. The full bridge inverter consists of four switches S_{1-4} connected in two legs where the switches $\mathrm{S}_{1,2}$ belong to 1st leg and switches $\mathrm{S}_{3,4}$ belong to 2nd leg. These switching devices are implemented using field-effect transistor (FETs) and the switching operation is controlled using pulses connected to the *Gate* terminal of FET.

The working principle of a phase-shifted full-bridge inverter can be understood by observing the switching waveforms and terminal voltages as illustrated in Figure 3.3. Switches in the same leg are turned on alternatively with a 50% duty cycle. In order to avoid short circuiting of the supply due to simultaneous turn-on during the transients, a dead time is applied where the both switches in the same leg are turned off (i.e. time periods $t_1 - t_2$, $t_3 - t_4$, $t_5 - t_6$ and $t_7 - t_8$). The phase difference between the two legs (indicated as δ in Figure 3.3) controls the pulse width (δ) of the output voltage waveform V_ab. The detailed description of the working principle of the full bridge inverter at different time intervals is given in Appendix A.1.

The output of the inverter is connected to LCC resonant network as illustrated

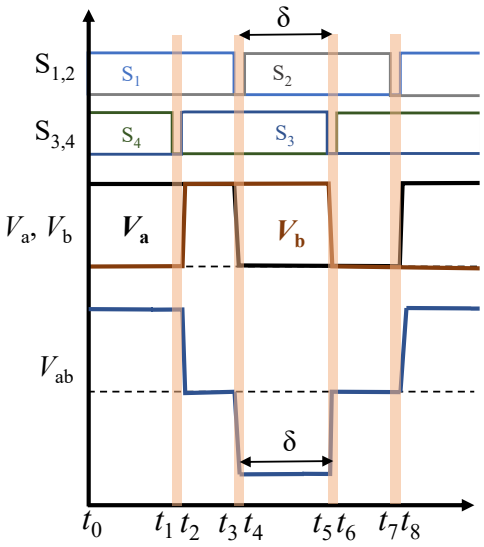

Figure 3.3 – Waveforms of a full-bridge converter.

in Figure 3.2. The input voltage of the LCC resonator V_{ab} is a square wave containing multiple harmonics, which can be written as

$$V_{\mathrm{ab}}(t) = \frac{4V_{\mathrm{DC}}}{n\pi} \sum_{n=1,3,5,\ldots}^{\infty} \frac{n\delta}{2} \sin\left(n\omega t\right) \tag{3.1}$$

It can be seen from Equation (3.1) that the input voltage contains odd multiples of the fundamental harmonic frequency (i.e. ω_0, $3\omega_0$, $5\omega_0$). The amplitude of the fundamental voltage can be varied by changing the phase difference between two legs δ. Next, the equivalent circuit analysis is performed to study the circuit behavior.

3.1.2 LCC compensation topology

LCC compensation topology is selected for this study due to its ability to supply constant current independent of load variations. Figure 3.2 shows the equivalent circuit of LCC resonant WPT system where L_{s}, C_{p} and C_{tx} are transmitter-side compensation inductor and capacitors respectively. L_{tx} is the transmitting coil inductance and L_{rx} is the receiving coil inductance. C_{rx} is the receiving side compensation capacitor, M is the mutual inductance between Tx and Rx and R_{L} is the load impedance. The coupling coefficient k is equal to $M/\sqrt{L_{\mathrm{tx}}L_{\mathrm{rx}}}$. The relationships between the components in the compensation network and the fundamental angular frequency ω_0 can be obtained as[26] is

given in Equation (3.2):

$$\begin{aligned} L_{\mathrm{s}}C_{\mathrm{p}} &= \frac{1}{\omega_0^2} \\ L_{\mathrm{tx}} - L_{\mathrm{s}} &= \frac{1}{\omega_0^2 C_{\mathrm{tx}}} \\ L_{\mathrm{rx}} &= \frac{1}{\omega_0^2 C_{\mathrm{rx}}} \end{aligned} \tag{3.2}$$

Using Kirchhoff's law, the below equations can be written to characterise the the circuit operation as,

$$\begin{aligned} V_{\mathrm{s},n} - (\mathrm{j}n\omega_0 L_{\mathrm{s}} + R_{\mathrm{s}})I_{\mathrm{s},n} + (I_{\mathrm{s},n} - I_{\mathrm{tx},n})\frac{1}{\mathrm{j}n\omega_0 C_{\mathrm{p}}} &= 0 \\ I_{\mathrm{tx},n}(\mathrm{j}n\omega_0 + \frac{1}{\mathrm{j}n\omega_0 C_{\mathrm{tx}}} + R_{\mathrm{tx}}) + \mathrm{j}n\omega_0 M I_{\mathrm{rx},n} - (I_{\mathrm{s},n} - I_{\mathrm{tx},n})\frac{1}{\mathrm{j}n\omega_0 C_{\mathrm{p}}} &= 0 \\ I_{\mathrm{rx},n}(\mathrm{j}n\omega_0 L_{\mathrm{rx}} + \frac{1}{\mathrm{j}n\omega_0 C_{\mathrm{rx}}} + R_{\mathrm{rx}} + R_{\mathrm{L}}) + \mathrm{j}n\omega_0 M I_{\mathrm{tx},n} &= 0 \end{aligned} \tag{3.3}$$

where ω_0 is the fundamental operating angular frequency, $V_{\mathrm{s},n}$ is the output voltage of the inverter, $I_{\mathrm{s},n}$ is the input voltage through L_{s}, I_{tx} is the current through the Tx coil, M is the mutual inductance between Tx and Rx and I_{rx} is the current through the Rx. Next, while solving for the currents through the coils and the components, the following some assumptions are made to simplify the analysis. Tx and Rx coils are identical therefore, L_{tx} = L_{rx} = L, losses in the coils and components are negligibly small compared to their reactance $R \approx 0$.

The currents in different branches for the n^{th} harmonic frequency can be written as,

$$\begin{aligned} I_{\mathrm{s},n} &= -\frac{nV_{\mathrm{s},n}(nR_{\mathrm{L}} + \mathrm{j}L\sigma\omega_0)}{\omega_0(\mathrm{j}nL_{\mathrm{s}}R_{\mathrm{L}} - (+M^2n^4)\sigma\omega_0 + L\sigma^2(-\mathrm{j}nR_{\mathrm{L}} + L\sigma\omega_0)}, \\ I_{\mathrm{tx},n} &= \frac{nV_{\mathrm{s},n}(\mathrm{j}nLR_{\mathrm{L}}\sigma + M^2n^4\omega_0 - L^2\sigma^2\omega_0)}{L_{\mathrm{s}}\omega_0(nR_{\mathrm{L}}(L_{\mathrm{s}} - L\sigma^2) + \mathrm{j}\sigma(M^2n^4 + L(L_{\mathrm{s}} - L\sigma^2))\omega_0)}, \\ I_{\mathrm{rx},n} &= \frac{\mathrm{j}Mn^3V_{\mathrm{s},n}}{-\mathrm{j}nR_{\mathrm{L}}(L_{\mathrm{s}} - L\sigma^2) + \sigma(M^2n^4 + L(L_{\mathrm{s}} - L\sigma^2))\omega_0} \end{aligned} \tag{3.4}$$

where $V_{\mathrm{s},n}$ = $4V_{\mathrm{dc}}/n\pi$ and harmonic content $n^2 - 1$ = σ. The currents at the

fundamental frequency (i.e. $n = 1$) can be written as

$$\begin{aligned} I_{\mathrm{s}} &= \frac{M^2 V_{\mathrm{s}}}{L_{\mathrm{s}}^2 R_{\mathrm{L}}}, \\ I_{\mathrm{tx}} &= -\mathrm{j}\frac{V_{\mathrm{s}}}{L_{\mathrm{s}}\omega_0}, \\ I_{\mathrm{rx}} &= -\frac{M V_{\mathrm{s}}}{L_{\mathrm{s}} R_{\mathrm{L}}} \end{aligned} \tag{3.5}$$

From Equation (3.5), we can observe that current through the Tx coil is always constant and it doesn't depend on mutual inductance M or load impedance R_{L}. Current through the compensation inductor L_{s} at the fundamental frequency ω_0 is a function of M^2/R_{L}. This means that in ideal conditions, the input current I_{s} is decreasing with the decrease of the mutual inductance or with increase of load impedance. Next, the output power considering fundamental harmonic component can be written as,

$$P_{\mathrm{out}} = I_{\mathrm{rx}}^2 R_{\mathrm{L}} \approx \frac{M^2 V_{\mathrm{s}}^2}{L_{\mathrm{s}}^2 R_{\mathrm{L}}} \approx I_{\mathrm{s}} V_{\mathrm{s}} \tag{3.6}$$

The efficiency of the WPTs system for fundamental harmonic can be written as follows,

$$\eta = \frac{I_{\mathrm{rx}}^2 R_{\mathrm{L}}}{I_{\mathrm{s}}^2 R_{\mathrm{s}} + I_{\mathrm{tx}}^2 R_{\mathrm{L}} + I_{\mathrm{rx}}^2 (R_{\mathrm{rx}} + R_{\mathrm{L}})} \tag{3.7}$$

Decreasing mutual inductance M means that Rx is moving away from Tx, and increasing R_{L} represents lower power requirement from the load. If multiple LCC tuned Tx coils are connected in parallel to the same power source, the input power from each Tx circuit is proportional to square of the mutual inductance between each Tx and Rx coils. This self-tuning characteristic is particularly useful for WPT with multiple Tx coils [26]. However, in practical situations, coils and other components have losses. The above characteristics may become invalid due to the effects of resistive losses. When the output power is below a certain threshold, power transfer becomes ineffective either because of very small coupling, or low power demand by the load, or both. If we can estimate the output power delivered to a load, we can deactivate ineffective Txs. Therefore, we propose a machine learning method to predict the output power only using transmitter-side measurements. For the rest of

the analysis we chose phase shift between two legs as $\delta = 180°$, and the fundamental frequency as 600 kHz. In the following section, we will discuss about the multi-transmitter systems and the activation or deactivation of Tx coils.

3.2 Multi-transmitter WPT system

Multi-transmitter WPT is based on multiple transmitter for simultaneously energize single or multiple receivers. In Figure 3.4, the equivalent circuit of a multi-transmitter WPT system is shown where q number of transmitter is visible. Similar to previous section, all the transmitters are tuned using LCC compensation and receiver circuit is tuned using series compensation. The component naming terminology is similar to that of Figure 3.2.

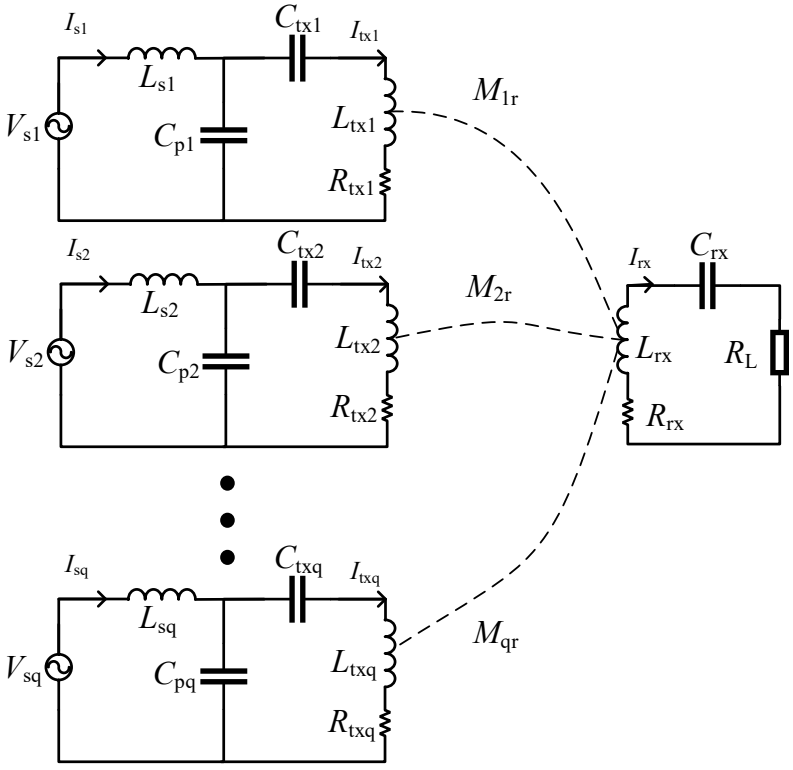

Figure 3.4 – The equivalent circuit of an LCC tuned multi-transmitter WPT system.

The working principle of multi-transmitter WPT system is similar to that of the single-transmitter WPT system. The resonance conditions for all Tx and

Rx are the same as single-Tx WPT system as defined in Equation (3.2). It is also assume that All the Tx coils are uncoupled from each other, which can be achieved by properly designing the Tx coil arrangement. For example, overlapped spiral shaped coils can be used to design the uncoupled Tx coils [18]. The mutual inductance between each transmitter and receiver are defined as $M_{1\mathrm{r}}$, $M_{2\mathrm{r}}$,...M_{qr}. The current equations in different branches can be extended for multi-transmitter systems for the fundamental frequency ($n = 1$) can be written as an extension of the Equation (3.5) as follows,

$$\begin{aligned} I_{\mathrm{s}} &= \frac{M_{r,m}^2 V_{s,m}}{L_{s,m}^2 R_{\mathrm{L}}}, \\ I_{\mathrm{tx}} &= -\mathrm{j}\frac{V_{s,m}}{L_{s,m}\omega_0}, \\ I_{\mathrm{rx}} &= \sum_{\text{m= active Txs}} -\frac{M_{r,m} V_{s,m}}{L_{s,m} R_{\mathrm{L}}} \end{aligned} \tag{3.8}$$

where, m is active Tx coil ranging from 1,2,3...,q.
The expressions for coil currents at different frequency harmonics are similar to that of single transmitter case as in Equation (3.4). The output power of a multi-transmitter systems can be derived from Equation (3.6) which is,

$$P_{\mathrm{out}} \approx \sum_{\text{m= active Txs}} \frac{M_{r,m}^2 V_{s,m}^2}{L_{\mathrm{s},m}^2 R_{\mathrm{L}}} \approx \sum_{\text{m= active Txs}} I_{\mathrm{s},m} V_{s.m} \tag{3.9}$$

Equation (3.9) is showing output power of multi-transmitter systems. For fundamental harmonic condition, input current I_{s} can be relate to output power P_{out} which is similar to single transmitter systems as shown in (3.6). From Equations (3.8) and (3.9), similar to single-transmitter WPT systems, I_{s} can be relate to find the output power required by the load R_{L} in multi-transmitter systems.
Multi-transmitter WPT systems can be described using single transmitter system point of view. Analysis of single transmitter systems can be used to explain the performance characteristics of multi-transmitter systems. Output power of multi-transmitter system depends on I_{s} as same as single transmitter systems. From Equations (3.5) and (3.8), both output power P_{out} and input current I_{s} depend on coupling k and load impedance R_{L}. When the output power is low (i.e. low k or high R_{L}) input current I_{s} will also be lower. However, for low power situation I_{tx} is still high as it doesn't depend on coupling k and load impedance R_{L} which will create unwanted electromagnetic exposure. To avoid this unwanted electromagnetic exposure, the Tx coils need to be turned off

that are not coupled with the receiver. When a receiver is closer to a particular Tx coil, the power transfer from the respective Tx coil is effective, whereas power transfer from farther away Tx coils are ineffective. Therefore, we should turn off farther away Tx coils to maintain high efficiency of the WPT system. Based on (3.5), we can easily detect farther away Tx coils by measuring the input current (current through L_{s}), as it is proportional to M^2/R_{L}, similar to the output power P_{out}. This allow us to use current I_{s} to estimate the delivered power to the receiver and classify the "turn-on" and "turn-off" state of the system. However, these derivations are written only for ideal case only considering fundamental harmonic frequency and when all the components are lossless. However, in practical situations, the above observations may vary significantly.

Therefore, single-transmitter WPT system can be used to characterise the output power estimation and classification of turn-on and turn-off decision for a particular Tx circuit. A Matlab based numerical approach is taken to understand the relation between different parameter in a practical scenario with realistic component losses and considering up to 7^{th} harmonics. The circuit shown in Figure 3.2 is analytically derived in Matlab to generate data contains contains information of the amplitudes and phases of different harmonic components of the input current I_{s}, the coupling coefficient (k), the load impedance (R_{L}), the output power (P_{out}), and the energy efficiency. Then the relation between I_{s}-P_{out} is observed which will be discussed later in the results section.

3.3 Estimating load impedance and coupling coefficient

The load impedance and the mutual inductance are important to evaluate the power requirement of the Rx. Load impedance can vary depending on the power demand of each receiver; for example, charging a laptop may need higher power than charging a mobile phone. Therefore, estimation of mutual inductance and load impedance using only transmitter-side measurements enables the understanding the receiver characteristics without any measurements from the receiver-side.

Frequency domain analysis is carried out to understand the effect of different operating frequencies rather than the resonance frequency. The resonance frequency of system is 600 kHz. An ac analysis on the circuit Figure 3.2 shows that, when the operating frequency is slightly lower (e.g., 590 kHz) or slightly

higher (e.g., 610 kHz) than the resonance frequency 600 kHz, then it is possible to distinguish between different harmonic phases and amplitudes of the input current I_{s} for different combination of R_{L} and coupling k. This lead us to use input current I_{s} phases and amplitudes at different frequencies to identify load impedance and coupling coefficients. In this approach, the 1^{st} and 3^{rd} harmonic components are considered as rest of them are negligibly small.
Similar to the estimation of output power, a Matlab based numerical approach is used to understand the relations of different parameters with load impedance and coupling coefficient. Next, a machine learning assisted method is proposed to estimate the loads impedance and coupling strengths using the input current I_{s} harmonics amplitudes and phases. The results are then validated using circuit simulations.

Chapter 4

Results and discussion

4.1 Simulation Setup

To understand the estimation of output power described in Section 3.1 a single-transmitter WPT system is simulated using LTspice. Two different WPT system configurations (System A and System B) have been studied to validate the proposed approach, and the system parameters are shown in the Table 4.1.

Table 4.1 – Simulation parameters details

Description	System A	System B
Tx Coil inductance (L_{tx})	6 μH	20 μH
Rx Coil inductance (L_{rx})	6 μH	20 μH
Resonant Inductor (L_{s})	2.5 μH	8 μH
Tx Coil internal resistance (R_{tx})	37.7 $m\Omega$	125.7 $m\Omega$
Rx Coil internal resistance (R_{rx})	37.7 $m\Omega$	125.7 $m\Omega$
Resonant inductor internal resistance (R_{s})	15.7 $m\Omega$	50.3 $m\Omega$
Input Voltage (V_{in})	10 V	
Switching Frequency (f_{s})	600 kHz	
Resonance Frequency (f_0)	600 kHz	
Load impedance (R_{L})	varied from 1 Ω to 200 Ω	
Coupling coefficient (k)	varied from 0.01 to 0.5	

The circuit is simulated by varying loads impedance and coupling coefficient, and the performance parameters including output voltage, output power and efficiency are observed. Load impedance (R_{L}) variation is chosen from 1 Ω to 200 Ω (spaced in logarithmic scale), and coupling coefficient (k) are chosen from 0.01 to 0.5 (spaced in linear scale) as illustrated in Table 4.1. From the simulation the amplitudes and phases of different harmonic components of the input current I_{s}, the coupling coefficient (k), the load impedance (R_{L}), the output power (P_{out}), and the energy efficiency are recorded.In the following section, these simulated outcome is studied using data analysis method and

then applied to machine learning algorithms to identify the most important features.

4.2 The proposed machine learning approach

In this section, we describe the proposed machine learning approach for the estimation of output power by only using the transmitter-side measurements.The simulation based data acquisition and training approach are discussed. For each combination of k and R_{L}, first seven harmonic components of the input current are recorded. A graphical representation between the RMS value of the current I_{s} and P_{out} is shown in Figure 4.1.

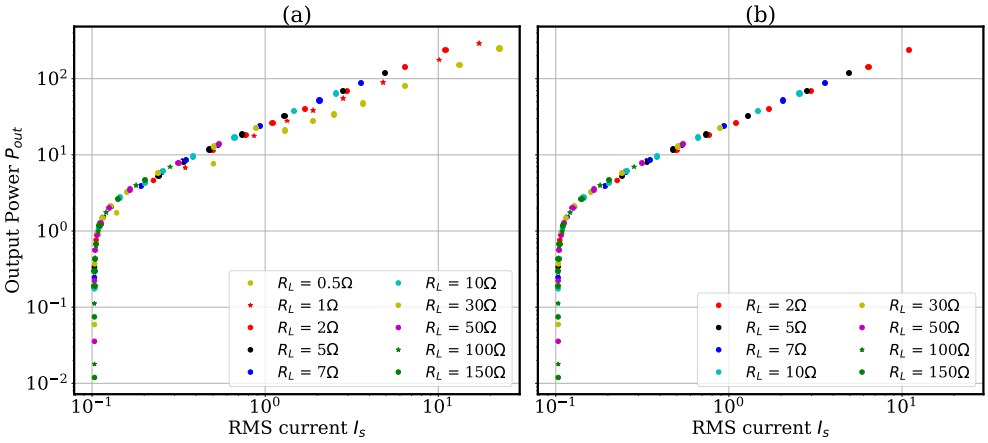

Figure 4.1 – Visualization of raw data set with and without outliers. (a) I_{s}-P_{out} profile containing outliers, and (b) I_{s}-P_{out} profile after removing outliers.

As shown in Figure 4.1a, the data set has outliers that can affect the performance of predictive models. The inter-quartile range method is applied to get rid of the outliers, as is shown in Figure 4.1b.
The feature importance for different measured variables is shown in Figure 4.2. The RMS value of the current I_{s} has the maximum importance for estimation of the output power. Apart from that, the amplitude of the fundamental harmonic ($A1$) also has high importance. The cleaned data set was then divided into training and testing sets. $80\ \%$ of the data was kept for training the machine learning models, and $20\ \%$ of the data was used for testing the performance of these models.

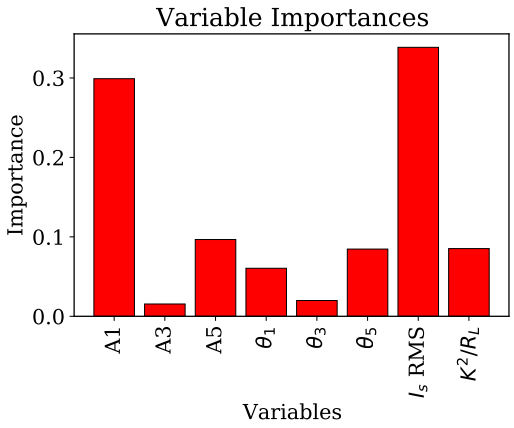

Figure 4.2 – Visualization of feature importance where A1, A3, and A5 are the magnitudes of the 1^{st} harmonic, 3^{rd} harmonic, and 5^{th} harmonic, respectively. θ_1, θ_3, and θ_5 are the phases of the 1st harmonic, 3^{rd} harmonic, and 5^{th} harmonic, respectively.

In this work, decision tree algorithm is used to predict a numerical target value P_{out} by using I_{s} RMS value as a feature. Random forest hyper-parameter tuning is done to achieve better prediction accuracy. SVR is used along with GridSearchCV parameter tuning. Table 4.2 contains parameters that are used in the decision-tree algorithm, random forest and support vector regressor.

Table 4.2 – Machine learning algorithms parameters [1, 2, 3]

Specifications	**Decision tree**	**Random forest**	**Support vector**	
maximum features:	None	['auto','sqrt']	Specifications	Details
max depth:	8	[5, 10, 15]	kernel:	['rbf','poly'],
min. samples leaf:	1	[1,2,4]	C:	[10,100,10000],
min. samples split:	2	[1,2,4]	gamma:	[1e-3,0.01,0.1,0.5],
random state:	42	42	epsilon:	[0.1,0.2,0.7],

4.3 Estimating output power

4.3.1 Analytical results

An analytical approach is taken by evaluating the circuit shown in Figure 3.2. A Matlab code is developed to analyse the different parameters of the circuit which will lead us to predict output power from transmitter-side measurement only. Equation stated in (3.3) are used to generate data which contains information of the amplitudes and phases of different harmonic components of

the input current I_s, the coupling coefficient (k), the load impedance (R_L), the output power (P_{out}), and the energy efficiency. Wide range of load impedance and coupling coefficient are used according to Table 4.1.
Referring to Section 3.1.2, simplified analytical equations are derived only considering the fundamental harmonic component of the current, and assuming the component losses are negligible. Therefore, (3.5) is not accurate enough for all the load impedance and coupling coefficient regions where higher-order harmonics are not very small. When the system become complex, considering all the lossless and other harmonics then it is analytically complex to predict output power from input current. Therefore, it is necessary to use a data-driven approach to accurately predict the output power only from the Tx-side measurements.

4.3.2 Simulation results

The switching frequency is chosen as 600 kHz for this simulation.

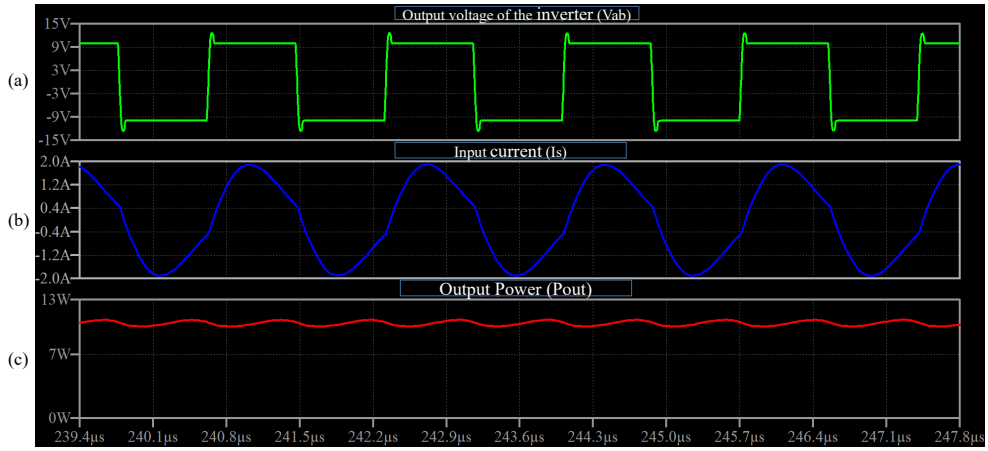

Figure 4.3 – Simulated waveforms for coupling k is 0.2 and load impedance R_L is 10Ω.(a) Output voltage of full-bridge converter V_{ab}, (b) Current I_s through inductor L_s, and (c) Output power P_{out} delivered to the load impedance R_L.

Simulation waveform when coupling coefficient k is 0.2 and load impedance R_L is 10 Ω are portrayed in Figure 4.3. Figure 4.3a is the output voltage (V_{ab}) of the full bridge circuit and 4.3b is the current through resonant inductor (L_s) and 4.3c is showing the output power delivered to the load.
Table 4.3 is showing the simulation outcome for 6 μH setup where three 1, 10 and 100 load impedance R_L values are chosen as well as three coupling coefficient 0.05, 0.1 and 0.4 are chosen. Table 4.3 contains the input power

Table 4.3 – Simulation results for different load impedance and coupling coefficients, where load impedance R_{L}, coupling coefficient k, input current I_{s}, input power P_{in}, output voltage V_{L}, output power P_{out} and efficiency η outcomes are shown.

$\mathrm{R_L}(\Omega)$	k	I_{s} (A)	P_{in} (W)	V_{L} (V)	P_{out} (W)	η (%)
1	0.05	0.53	12.42	3.06	9.34	75.20
1	0.1	1.47	40.85	5.89	34.78	85.15
1	0.4	20.99	568.4	21.65	468.57	82.43
10	0.05	0.38	9.01	3.23	1.04	11.56
10	0.1	0.41	9.59	6.45	4.15	43.32
10	0.4	2.39	65	24.37	59.36	91.32
100	0.05	0.38	8.97	3.25	0.105	1.17
100	0.1	0.38	9	6.49	0.42	4.68
100	0.4	0.45	10.45	25.85	6.68	63.97

P_{in}, RMS current I_{s}, output power P_{out}, output voltage V_{L}, and efficiency η for different combination of R_{L} and k. It can be observed from Table 4.3 that for smaller value of load impedance, the output power is high and for larger value of coupling, the output power is high, which can be justified from (3.6). Similarly, for smaller value of load the input current is high where for larger value of coupling the input current is high, which can be justified from (3.5). To support this simulated study, a machine learning study is carried out in the following section.

ML results

The main objective of the machine learning prediction is to estimate the output power P_{out} using the Tx-side measurements. After cleaning the data, feature importance are ranked as shown in Figure 4.2, in order to understand the suitable feature(s) for the prediction of P_{out}. We can see from Figure 4.2 that the RMS value of I_{s} has the highest importance for prediction of P_{out}. In addition, measurements of RMS current are relatively straightforward compared to other considered features. Therefore, we use RMS of I_{s} for the prediction. Train data points are fed into the selected algorithms to train the models and then evaluated using the test points. The model performances are compared in Table 4.4. The results show that only the random forest algorithm gives acceptable accuracy above $80\ \%$ average accuracy.
In Figure 4.4, all the test points percentage error are shown for the random forest, decision tree, and support vector machine algorithms. Random forest has less than $20\ \%$ error which is the minimum error among the other algorithms for both systems. Random forest has the largest run time of 43.51 seconds for the training. However, this run time is not a critical concern for

Table 4.4 – ML models performance for estimating output power

Model Name	Average Accuracy (%)	Run Time (seconds)
Random Forest	83.01	43.51
Decision Tree	43.07	0.0015
Support Vector	69.88	4.41

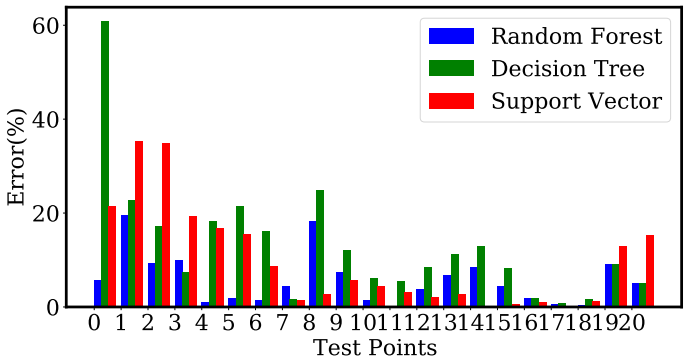

Figure 4.4 – Visualization of percentage error for system A for three different machine learning algorithms

WPT applications as the training is a one-time action. Therefore, we chose random forest algorithm for the subsequent analysis.

4.3.3 Experimental results

An experiment is conducted to validate the simulation results. Two coils having inductance of $5.6\ \mu$H are designed along with the resonant inductor L_{s} of $2.15\ \mu$H. TIC2000 digital signal processor is used to generate the gate pulses of the switches in full-bridge converter. A current sensor is used to find the RMS current through the resonant inductor L_{s}. As shown in Figure 4.6, a 3D printed structure is created for the transmitter and receiver coils. A full bridge converter is designed and developed which is connected with a LCC resonator circuit. A range of load impedance R_{L} were selected between $2\ \Omega$ to $100\ \Omega$. The position of the receiver is changed to obtain the results for different coupling strengths.
Th parameters of the experimental setup are shown in Table 4.5. As discussed in 4.3.2, the experimental study shows that for smaller value of load the output power is high where for larger value of coupling the output power is high, which can be justified from (3.6). In Figure 4.7, the output waveforms of the experimental study is shown for different loads resistances. This output waveform includes the square wave that is generated by the inverter, the input

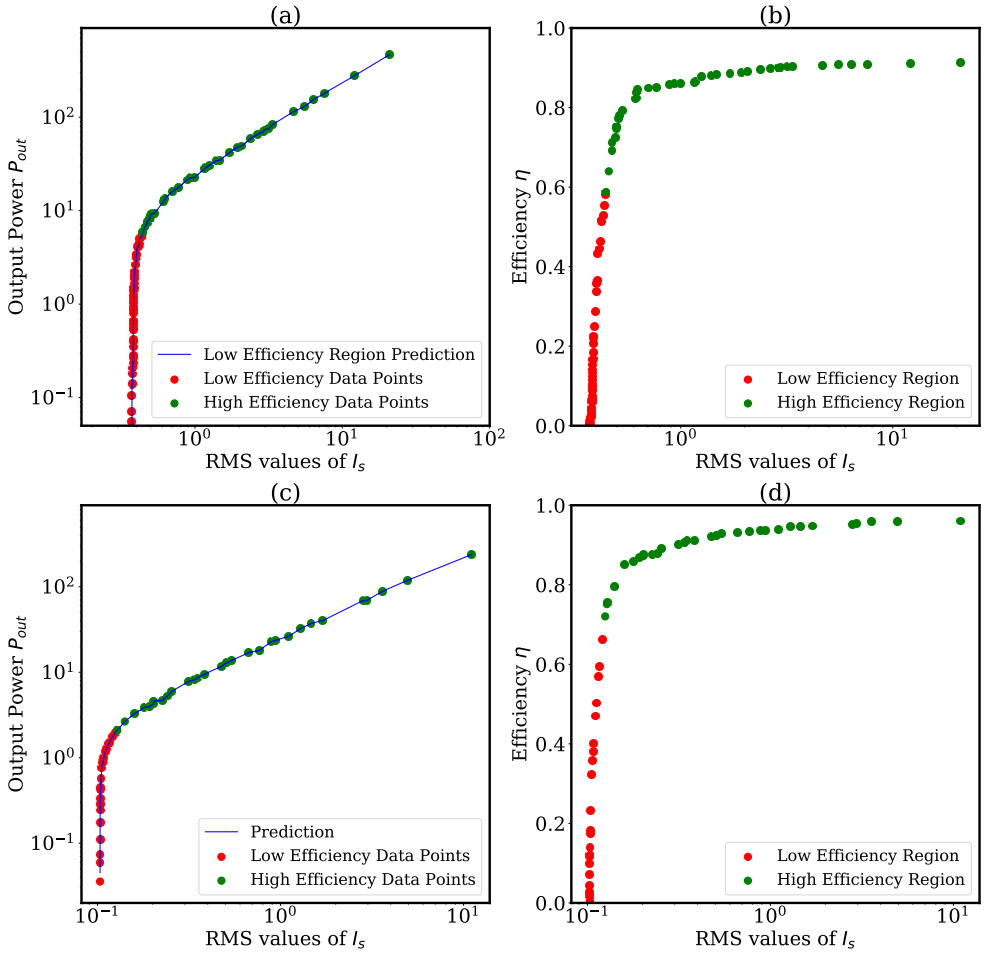

Figure 4.5 – Output power and efficiency variations with respect to RMS value of I_s. (a) fitted predictive line of output power for system A, (b) efficiency of system A, (c) fitted predictive line of output power for system B, and (d) efficiency of system B. Classification of "turn off" and "turn on" regions are indicated in different colors.

current I_s and output voltage V_L.

4.3.4 Discussion

Figure 4.8 is illustrating the outcomes of analytical, simulation and experimental study on the circuit shown in Figure 3.2. In all the results, it can be seen that input current I_s can be used to predict the output power P_{out}. All the graphs have a similar trend. Table 4.1 is containing the parameter specification that is used for this study. From Figure 4.8a, input current I_s RMS values are plotted

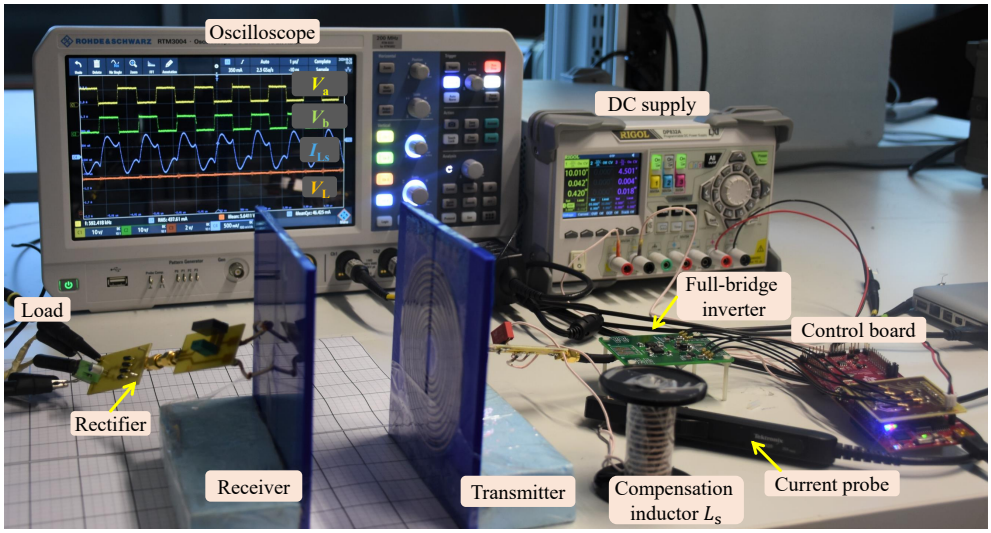

Figure 4.6 – The experimental setup.

Table 4.5 – Experimental results for different load impedance and coupling coefficients, where load impedance R_{L}, coupling coefficient k, input current I_{s}, input power P_{in}, output voltage V_{L}, output power P_{out} and efficiency η outcomes are shown.

R_{L} (Ω)	Position X,Y (mm)	I_{s} (A)	P_{in} (W)	V_{L} (V)	P_{out} (W)	η (%)
2	10,10	3.72	30.5	6.98	24.36	79.87
2	20,10	2.45	21.85	5.47	14.96	69.33
10	10,0	1.335	12.36	10.34	10.69	86.48
10	10,10	1.17	10.792	9.67	9.35	86.65
100	10,0	0.242	1.802	11.835	1.40	77.77
100	10,10	0.225	1.632	11.16	1.25	76.31

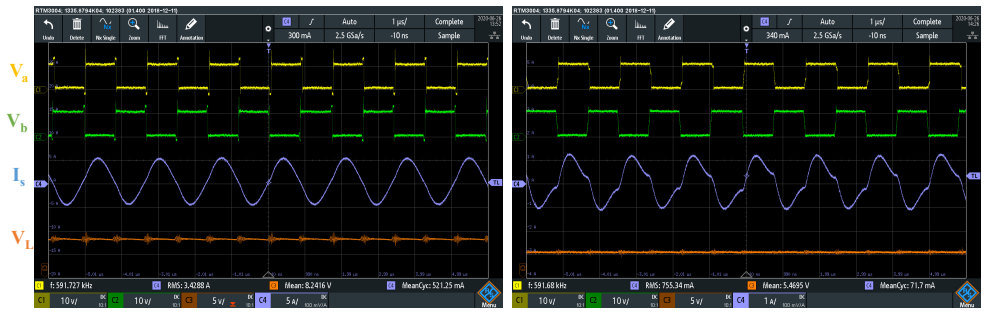

(a) R_L=3Ω (b) R_L=5Ω

Figure 4.7 – Output waveforms of the experimental study where inverter output V_a, V_b, input current I_{s} and output voltage V_L are shown.

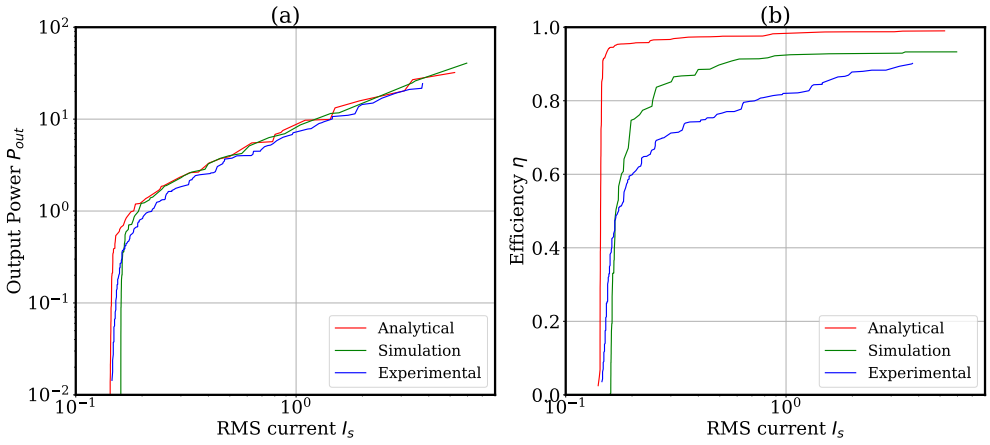

Figure 4.8 – The comparison of analytical, simulation, and experimental results for (a) output power and (b) efficiency. The analytical profiles are generated from equations 3.6 and 3.7.

.

against output power P_{out} which contains all the presentation of analytical, simulated and experimental profile. This I_{s}-P_{out} profile is showing that theoretical results match with simulation and experimental results. Figure 4.8b is showing I_{s}-η profile for theoretical, simulated and experimental results. The theoretical efficiency η slightly defers from simulated and experimental efficiency. This deviation in efficiency profile is because losses in the full-bridge converter are not considered in the analytically calculated efficiency.
The output power (P_{out}) and efficiency variation against RMS current I_{s} graphs are shown in Figure 4.5 for both system A and B. As seen in Figure 4.5(a) and (c), the P_{out} profile has a linear part and a polynomial part. The high-power region is mostly in the linear part. We can also notice from Figure 4.5(b) and (d) that efficiency is high when the system is operating in the high-power region. To this end, the random sampling consensus (RANSAC) algorithm is used to identify the high-efficiency region by estimating the linearity of the $P_{\text{out}} - I_{\text{s}}$ curve. RANSAC algorithm is a well-known method in machine learning to identify linearity and outliers [48]. A cut-off point is identified using RANSAC algorithm which is the determinant of turning-on or off the transmitter as illustrated in Figure 4.5. We can see that the turn-on region has efficiency higher than 60 %, which verifies the efficacy of the proposed classification. Random forest regressor is used to predict the output power P_{out} from the RMS value of I_{s}, then random forest classifier to identify whether the system is working in the high-efficiency regime or not. In this way, we can estimate the output power and decide whether we should activate

or deactivate the Tx coil only based on I_s measurements. This method can be particularly useful in multi-transmitter WPT systems when a receiver is closer to a particular Tx coil, the power transfer from the respective Tx coil is effective, whereas power transfer from farther away Tx coils are ineffective. Therefore, we should turn-off farther away Tx coils to maintain high efficiency of the WPT system.

4.4 Estimating load impedance and coupling coefficient

4.4.1 Analytical results

An analytical study on estimating load impedance and coupling coefficient has been done using Matlab. A Matlab code is developed to analyse the different parameters of the circuit shown in Figure 3.2 which will help to distinguish between load impedance and coupling coefficient. An ac sweep from 100 kHz to 1 MHz and observed the effect of different harmonic components on identifying load impedance and coupling coefficient.

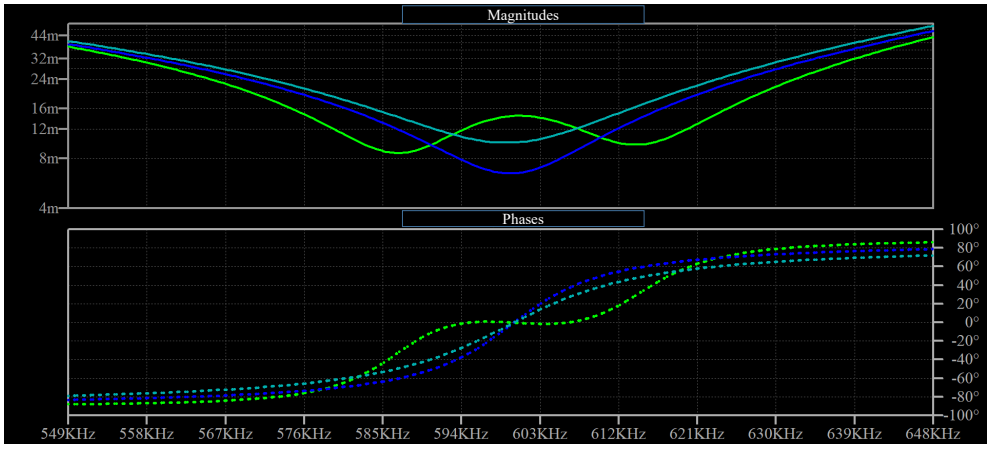

Figure 4.9 – Frequency domain analysis of magnitude and phases of input current for different load impedance.

For example, Figure 4.9 shows frequency response of I_s from 100 kHz to 1 MHz where magnitude and phases of input current I_s can be seen. This is plot for load impedance R_L 1,10,100 and coupling factors k of 0.05, 0.1, 0.4. As the WPT system is tuned for resonance at 600 kHz, the magnitudes are distinguishable at resonance frequency but all the phase angles are zero

for all the combination of load impedance and coupling coefficients. Only magnitudes alone cannot be used to estimate both the load impedance and coupling coefficient. If the system is working at slightly lower (e.g. at 590 kHz) or slightly higher (e.g. at 610 kHz) frequency than resonance frequency, then the magnitudes and phases are distinguishable. However, it is not accurate to use these analytical solutions of the currents to estimate the load impedance due to the non-idealities and non-linearities in a practical WPT system. Therefore, machine learning can be utilized to find a relation between transmitter side parameters and the system configurations (i.e. load impedance and coupling coefficient).

4.4.2 Simulation results

A LTspice simulation has been done to study the behaviour of load impedance and coupling coefficient in relation with transmitter side parameters. In the simulation, same range of load impedance and coupling coefficient mentioned in 4.1.

Figure 4.10 shows the relation between 1st harmonic with load impedance and coupling coefficient. In Figure 4.10a, 1st harmonic magnitude can easily distinguish different coupling coefficient when the coupling is greater than 0.1. Similarly, as shown in Figure 4.10b, the 1st harmonic magnitude can also be used to estimate load impedance values.With regards to the phase angles, (results are illustrated in Figure 4.10c and d), 1st harmonic phase can be more effective in estimating both coupling coefficient and load impedance values. This simulation results show that 1st harmonic magnitude and phase angle can be useful to estimate load impedance and coupling coefficient.
Figure 4.11 illustrates the relation between 3rd harmonic of I_{s} with load impedance and coupling coefficient. We can see that 3rd harmonic magnitude can easily distinguish different coupling coefficients only if the coupling is greater than 0.2 which means that 3rd harmonic magnitude is not helpful to estimate coupling coefficient lower than 0.2. Besides, we can see from Figure 4.11a that the 3rd harmonic magnitude is not effective to estimate load impedance. On the other hand, the 3rd harmonics phase angles (refer Figure 4.11c and d) can be more effective than 3rd harmonic magnitude in estimating both couplings and load impedance values. This simulation results show that 3rd harmonic phase is coherent to estimate load impedance and coupling coefficient.

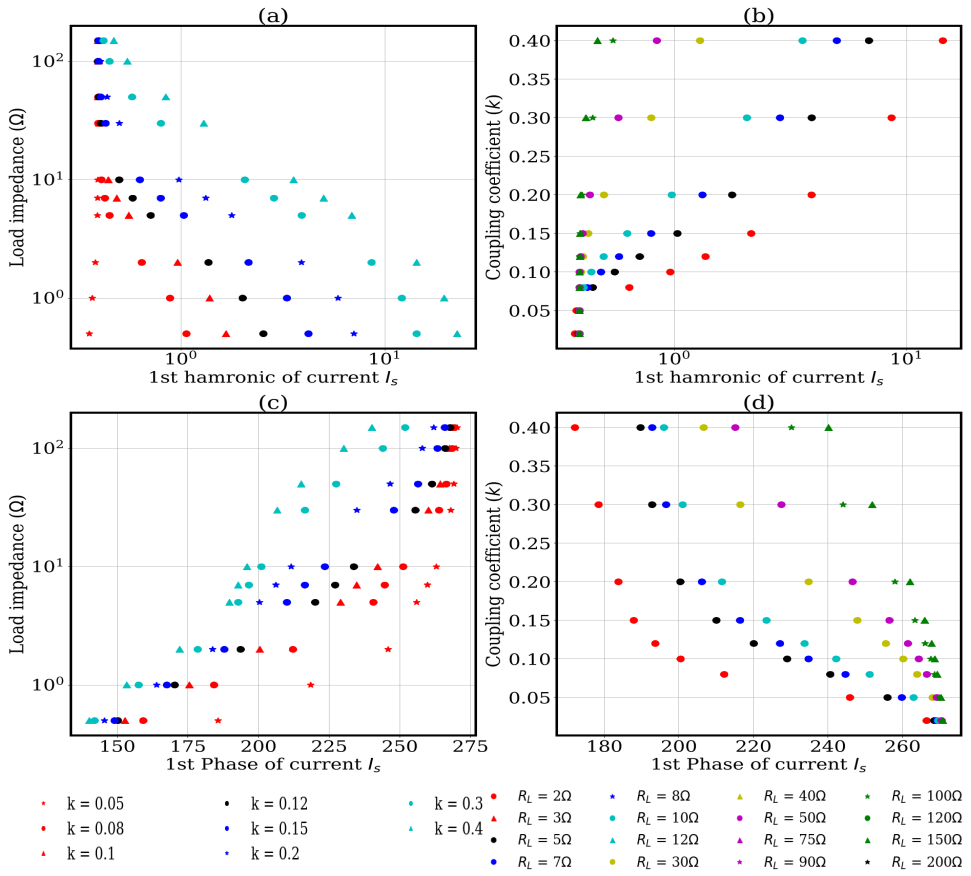

Figure 4.10 – Visualisation of 1^{st} harmonic components of input current I_s with load impedance and coupling coefficient. (a) 1^{st} harmonic magnitude against load impedance for different coupling coefficient values (b) 1^{st} harmonic magnitudes against coupling coefficient values for different load impedances, (c) 1^{st} harmonic phases against load impedance for different coupling coefficient values, and (d) 1^{st} harmonic phases against coupling coefficient values for different load impedances.

ML results

The objective of using machine learning is to study the transmitter-side parameters importance that can be utilized to predict load impedance and coupling coefficient. From the simulation results, it can be understood that input current I_s harmonic components and the RMS values can be used to estimate load impedance and coupling coefficient. In order to further validate the influence of different parameters, the feature importance study is performed for each transmitter-side variables, as illustrated in Figure 4.12. Three different

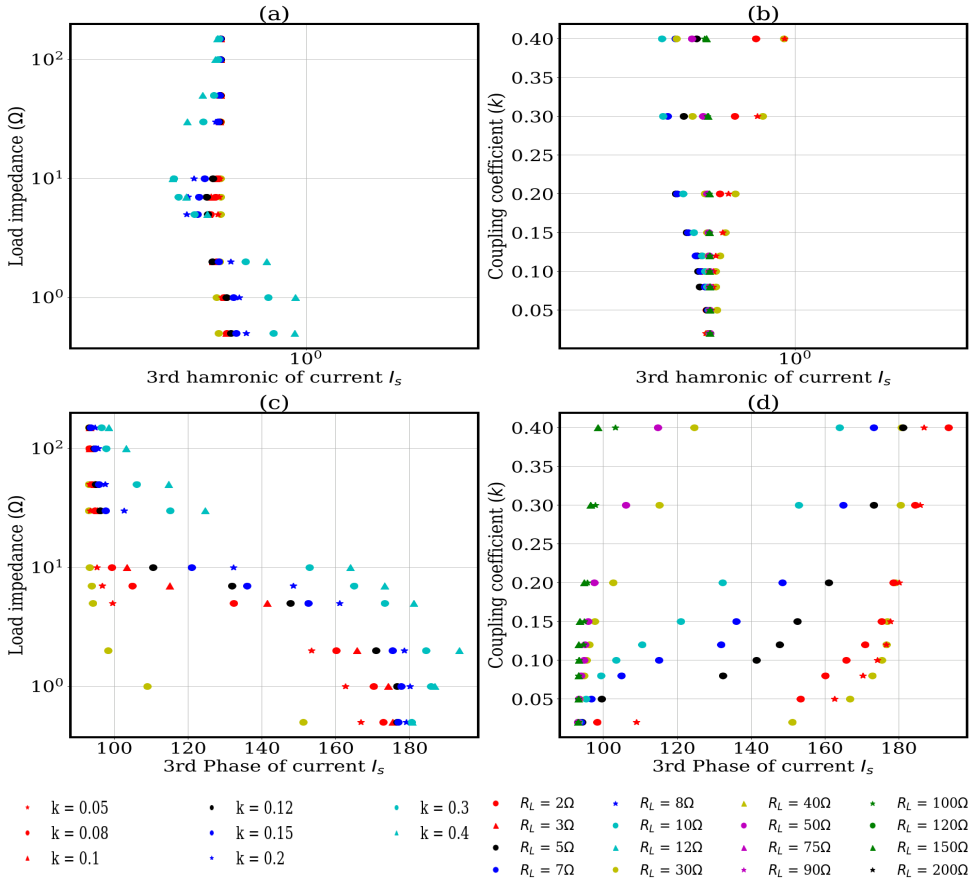

Figure 4.11 – Visualisation of 3rd harmonic components of input current I_s with load impedance and coupling coefficient. (a) 3^{rd} harmonic magnitude against load impedance for different coupling coefficient values, (b) 3^{rd} harmonic magnitudes against coupling coefficient values for different load impedances, (c) 3^{rd} harmonic phases against load impedance for different coupling coefficient values, and (d) 3^{rd} harmonic phases against coupling coefficient values for different load impedances.

frequencies 590 kHz, 600 kHz and 610 kHz are considered for this study. It can be understood that 1st harmonic phase of 590 kHz and 1st harmonic phase of 610 kHz of input current I_s has the most importance estimating load impedance and coupling coefficient. Apart from this, 3rd harmonic phase of 610 kHz for I_s also has high importance. These observations are inline with the discussion in the previous section.

In Table 4.6, average percentage errors are shown for three different machine learning algorithms, the random forest, adabooster with random forest, and

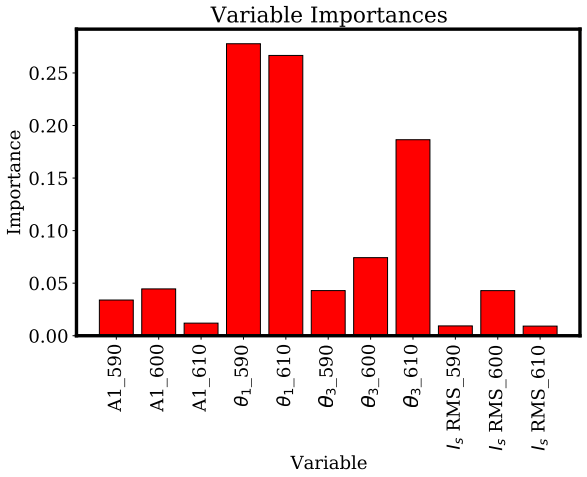

Figure 4.12 – Features importance for estimating load impedance and coupling coefficient where $A1_{590}$, $A1_{600}$, $A1_{610}$, are the magnitudes of the 1^{st} harmonic, $\theta_{1_{590}}$, $\theta_{1_{610}}$, $\theta_{3_{590}}$, and $\theta_{3_{610}}$ are the phases of the 1^{st} harmonic, 3^{rd} harmonic, RMS of input current I_{s} also shown for frequencies at 590 kHz, 600 kHz and 610 kHz respectively.

Table 4.6 – Average accuracy (%) for estimating load impedance and coupling coefficient

Model Name	**Coupling coefficient** k	**Load impedance** R_{L}
Random Forest	94.81%	75.72%
Adabooster with RF	90.53%	77.05%
XGBboost	90.05%	69.62%

XGBboost. Random forest has less than 6% error when its about predicting the coupling coefficient, which is the minimum error among the other algorithms for both systems. In terms of predicting load impedance values, adaboost with RF has 22.95 % average error which is lower than other two algorithms.

4.4.3 Discussion

The simulation results in Figure 4.10 and Figure 4.11 show that the relation between 1^{st} and 3^{rd} harmonic contents with load impedance and coupling coefficient. It is clear from the results that the fundamental harmonic magnitude and phase along with 3^{rd} harmonic phase can be utilized in estimating the load impedance and coupling coefficient. Moreover, random forest algorithm is used to identify the most important features that would lead us to estimate the load impedance and coupling coefficient. In Figure 4.12, shows that 1^{st} and

3^{rd} harmonic phase at frequencies at 590 kHz and 610 kHz has the maximum importance in estimating load impedance and coupling coefficient which is equivalent to the simulation outcomes. Thus, random forest, adabooster with RF and XGboost machine learning algorithms are used to estimate load impedance and coupling coefficient using those features. Among which, random forest shows decent outcome in estimating load impedance impedance and coupling coefficient. Therefore, it is clear from the above discussion that machine learning assisted methods can be used to accurately predict coupling coefficient (with an average error of 6%) while load impedance can be predicted with a reasonable accuracy (with an average error of 22%).
The estimation of load impedance and coupling coefficient will allow us to understand the the position of the receiver as well as the power requirement of the load. In a multi-transmitter WPT system, for a given load when the position of a receiver is varying the power delivered to the load will vary with it. As discussed earlier, when a receiver is closer to a particular transmitter coil, the power transfer from the respective transmitter coil is effective, whereas power transfer from farther away transmitter coils are ineffective. By using the proposed method estimation of load impedance and coupling coefficient, it is easily possible to understand the position of the receiver and based on the estimation the nearby transmitters can be activated and farther away transmitters can be turned off. The possible improvements and future directions of the proposed study is discussed in the following chapter.

Chapter 5

Conclusions and future work

5.1 Conclusions

Coupling and load impedance variations have significant effects on the efficiency and system characteristics of wireless power transfer devices. In this project, we have proposed a simple machine learning approach to predict the output power of the receiver by observing the transmitter-side parameters. Also, machine learning approach is used to estimate the load impedance and coupling coefficient by taking only transmitter-side measurements. Feature importance method is utilized to find the optimal feature to predict the output power and identify the load impedance and coupling coefficient. Several machine learning algorithms including random forest, decision tree, and support vector regressor have been evaluated. Among these, the random forest algorithm has been found to offer the best accuracy of output power predictions. Random forest classification has been used to classify the turn-on and turn-off regions for the transmitting coils based on efficiency considerations. Multi-output regression method is employed to estimate load impedance and coupling coefficient. Random forest based multi-output regression has the minimum average error to estimate load impedance and coupling coefficient. On the other hand, adabooster based random forest shows less error to estimate load impedance values.
To enable free positioning of the load, knowing the coupling strength is crucial, and the random forest method has the minimum error to do that. For this reason, random forest is most suitable for the goals of this project. The method proposed in this thesis uses only the transmitter-side parameters and, therefore, no extra sensors or feedback loops are required. The proposed method can be useful for optimal activation of multi-transmitter WPT systems. The results

of this work can be used to dynamically track the load status and the coupling of the transmitting coil with the receiving coil in a WPT system that is LCC-S compensated. In addition, only measurement of transmitter parameters is required, which makes the proposed process simple and straightforward.

5.2 Limitations

This work is limited to single Tx-Rx and multi-Tx and single-Rx systems. The developed experimental setup allows estimations of the output power only, as only the input current RMS is needed to predict the output power. Measuring RMS current is straightforward, as there are many sensors that can measure RMS current. However, estimating load impedance and coupling coefficient requires measuring harmonic components of the current, which is a difficult task. Due to experimental complexity and time limitation, this project work does not include experimental study of estimation of load impedance and coupling coefficient. This work is carried out using simple and efficient machine learning algorithms, however, some higher order algorithms can be chosen by increasing the data-set to perform the study.

5.3 Future work

This work can be extended for multi-receiver WPT systems. When considering the multi-receiver condition, the system becomes more complex. Further study can be done to develop a similar method as in this work to predict the output power and estimate the load impedance and coupling coefficient. Also, the activation or deactivation of the transmitter based on efficiency characteristics can be studied. The alignment of the receiver can be studied for both single- and multi-Tx-Rx systems.

References

[1] RandomForestRegressor — scikit-learn 0.23.2 documentation. [Online]. Available: https://scikit-learn.org/stable/modules/generated/sklearn.ensemble.RandomForestRegressor.html

[2] SVR — scikit-learn 0.23.2 documentation. [Online]. Available: https://scikit-learn.org/stable/modules/generated/sklearn.svm.SVR.html

[3] DecisionTreeRegressor — scikit-learn 0.23.2 documentation. [Online]. Available: https://scikit-learn.org/stable/modules/generated/sklearn.tree.DecisionTreeRegressor.html

[4] N. Tesla, "High frequency oscillators for electro-therapeutic and other purposes," vol. 87, no. 7, p. 1282. doi: 10.1109/JPROC.1999.771079. [Online]. Available: http://ieeexplore.ieee.org/document/771079/

[5] S. Assawaworrarit, X. Yu, and S. Fan, "Robust wireless power transfer using a nonlinear parity–time-symmetric circuit," vol. 546, no. 7658, pp. 387–390. doi: 10.1038/nature22404. [Online]. Available: http://www.nature.com/articles/nature22404

[6] Y. Luo, Y. Yang, S. Chen, and X. Wen, "A frequency-tracking and impedance-matching combined system for robust wireless power transfer," vol. 2017, pp. 1–13. doi: 10.1155/2017/5719835. [Online]. Available: https://www.hindawi.com/journals/ijap/2017/5719835/

[7] M. Fu, T. Zhang, C. Ma, and X. Zhu, "Efficiency and optimal loads analysis for multiple-receiver wireless power transfer systems," vol. 63, no. 3, pp. 801–812. doi: 10.1109/TMTT.2015.2398422. [Online]. Available: http://ieeexplore.ieee.org/document/7039263/

[8] J. Casanova, "A loosely coupled planar wireless power system for multiple receivers," vol. 56, no. 8, pp. 3060–3068. doi:

10.1109/TIE.2009.2023633. [Online]. Available: http://ieeexplore.ieee.org/document/5067306/

[9] D. Ahn and S. Hong, "Effect of coupling between multiple transmitters or multiple receivers on wireless power transfer," vol. 60, no. 7, pp. 2602–2613. doi: 10.1109/TIE.2012.2196902. [Online]. Available: http://ieeexplore.ieee.org/document/6192319/

[10] A. K. RamRakhyani, S. Mirabbasi, and M. Chiao, "Design and optimization of resonance-based efficient wireless power delivery systems for biomedical implants," vol. 5, no. 1, pp. 48–63. doi: 10.1109/TBCAS.2010.2072782. [Online]. Available: http://ieeexplore.ieee.org/document/5595028/

[11] "A low-operating-voltage wireless intermediate-range scheme for energy and signal transmission by magnetic coupling for implantable devices," vol. 3, no. 1, pp. 242–251. doi: 10.1109/JESTPE.2014.2314388. [Online]. Available: http://ieeexplore.ieee.org/document/6780635/

[12] C. C. Mi, "Wireless power transfer for electric vehicle applications," vol. 3, no. 1, pp. 4–17. doi: 10.1109/JESTPE.2014.2319453. [Online]. Available: http://ieeexplore.ieee.org/document/6804648/

[13] J. Yin, D. Lin, C. K. Lee, T. Parisini, and S. Y. Hui, "Front-end monitoring of multiple loads in wireless power transfer systems without wireless communication systems," vol. 31, no. 3, pp. 2510–2517. doi: 10.1109/TPEL.2015.2426313. [Online]. Available: https://ieeexplore.ieee.org/document/7094285/

[14] D.-W. Seo, J.-H. Lee, and H. Lee, "Integration of resonant coil for wireless power transfer and implantable antenna for signal transfer," vol. 2016, pp. 1–7. doi: 10.1155/2016/7101207. [Online]. Available: http://www.hindawi.com/journals/ijap/2016/7101207/

[15] K. Kandasamy, D. M. Vilathgamuwa, U. K. Madawala, and K.-J. Tseng, "Inductively coupled modular battery system for electric vehicles," vol. 9, no. 3, pp. 600–609. doi: 10.1049/iet-pel.2014.0553. [Online]. Available: https://digital-library.theiet.org/content/journals/10.1049/iet-pel.2014.0553

[16] S. Choi, J. Huh, W. Y. Lee, S. W. Lee, and C. T. Rim, "New cross-segmented power supply rails for roadway-powered electric vehicles,"

vol. 28, no. 12, pp. 5832–5841. doi: 10.1109/TPEL.2013.2247634. [Online]. Available: http://ieeexplore.ieee.org/document/6470688/

[17] N. Korakianitis, G. A. Vokas, and G. Ioannides, "Review of wireless power transfer (WPT) on electric vehicles (EVs) charging." doi: 10.1063/1.5138558 p. 020072. [Online]. Available: http://aip.scitation.org/doi/abs/10.1063/1.5138558

[18] P. Jayathurathnage and F. Liu, "Optimal excitation of multi-transmitter wireless power transfer system without receiver sensors," in *2019 IEEE PELS Workshop on Emerging Technologies: Wireless Power Transfer (WoW)*. IEEE. doi: 10.1109/WoW45936.2019.9030611. ISBN 978-1-5386-7514-4 pp. 25–28. [Online]. Available: https://ieeexplore.ieee.org/document/9030611/

[19] Q. Xu, H. Wang, Z. Gao, Z.-H. Mao, J. He, and M. Sun, "A novel mat-based system for position-varying wireless power transfer to biomedical implants," vol. 49, no. 8, pp. 4774–4779. doi: 10.1109/TMAG.2013.2245335. [Online]. Available: http://ieeexplore.ieee.org/document/6466385/

[20] S. Jeong, J. Bito, and M. M. Tentzeris, "Design of a novel wireless power system using machine learning techniques for drone applications," in *2017 IEEE Wireless Power Transfer Conference (WPTC)*. IEEE. doi: 10.1109/WPT.2017.7953890. ISBN 978-1-5090-4585-3 pp. 1–4. [Online]. Available: http://ieeexplore.ieee.org/document/7953890/

[21] Faraday's law of induction | physics. [Online]. Available: https://www.britannica.com/science/Faradays-law-of-induction

[22] Ampère's law. [Online]. Available: https://www.britannica.com/science/Amperes-law

[23] C. C. Mi, G. Buja, S. Y. Choi, and C. T. Rim, "Modern advances in wireless power transfer systems for roadway powered electric vehicles," vol. 63, no. 10, pp. 6533–6545. doi: 10.1109/TIE.2016.2574993. [Online]. Available: http://ieeexplore.ieee.org/document/7491313/

[24] G. Monti, L. Corchia, E. De Benedetto, and L. Tarricone, "A wearable wireless energy link for thin-film batteries charging," vol. 2016, pp. 1–9. doi: 10.1155/2016/9365756. [Online]. Available: http://www.hindawi.com/journals/ijap/2016/9365756/

[25] T. Kan, R. Mai, P. P. Mercier, and C. C. Mi, "Design and analysis of a three-phase wireless charging system for lightweight autonomous underwater vehicles," vol. 33, no. 8, pp. 6622–6632. doi: 10.1109/TPEL.2017.2757015. [Online]. Available: https://ieeexplore.ieee.org/document/8052169/

[26] C. Xiao, D. Cheng, and K. Wei, "An LCC-c compensated wireless charging system for implantable cardiac pacemakers: Theory, experiment, and safety evaluation," vol. 33, no. 6, pp. 4894–4905. doi: 10.1109/TPEL.2017.2735441. [Online]. Available: https://ieeexplore.ieee.org/document/8000589/

[27] S. Shalev-Shwartz and S. Ben-David, *Understanding machine learning: from theory to algorithms*. ISBN 978-1-107-29801-9 OCLC: 1135996373.

[28] J. M. Z. H, J. Hossen, S. Sayeed, C. Ho, T. K, A. Rahman, and E. Arif, "A survey on cleaning dirty data using machine learning paradigm for big data analytics," vol. 10, no. 3, p. 1234. doi: 10.11591/ijeecs.v10.i3.pp1234-1243. [Online]. Available: http://www.iaescore.com/journals/index.php/IJEECS/article/view/12097

[29] C. Guo and F. Berkhahn, "Entity embeddings of categorical variables." [Online]. Available: http://arxiv.org/abs/1604.06737

[30] L. Rokach and O. Maimon, "Decision trees," in *Data Mining and Knowledge Discovery Handbook*, O. Maimon and L. Rokach, Eds. Springer-Verlag, pp. 165–192. ISBN 978-0-387-24435-8. [Online]. Available: http://link.springer.com/10.1007/0-387-25465-X_9

[31] T. Evgeniou and M. Pontil, "Support vector machines: Theory and applications," in *Machine Learning and Its Applications*, G. Paliouras, V. Karkaletsis, and C. D. Spyropoulos, Eds. Springer Berlin Heidelberg, vol. 2049, pp. 249–257. ISBN 978-3-540-42490-1 978-3-540-44673-6. [Online]. Available: http://link.springer.com/10.1007/3-540-44673-7_12

[32] A. Miller, *Machine learning: the beginner's guide to algorithms, neural networks, random forests and decision trees made simple*. ISBN 978-1-978046-86-3 OCLC: 1086605835.

[33] J. Bergstra and Y. Bengio, “Random search for hyper-parameter optimization,” vol. 13, no. 10, pp. 281–305. [Online]. Available: http://jmlr.org/papers/v13/bergstra12a.html

[34] H. Borchani, G. Varando, C. Bielza, and P. Larrañaga, “A survey on multi-output regression: Multi-output regression survey,” vol. 5, no. 5, pp. 216–233. doi: 10.1002/widm.1157. [Online]. Available: http://doi.wiley.com/10.1002/widm.1157

[35] A. P. Sample, D. A. Meyer, and J. R. Smith, “Analysis, experimental results, and range adaptation of magnetically coupled resonators for wireless power transfer,” vol. 58, no. 2, pp. 544–554. doi: 10.1109/TIE.2010.2046002. [Online]. Available: http://ieeexplore.ieee.org/document/5437250/

[36] L. Sun, M. Sun, D. Ma, and H. Tang, “Detecting load resistance and mutual inductance in series-parallel compensated wireless power transfer system based on input-side measurement,” vol. 2018, pp. 1–6. doi: 10.1155/2018/2094637. [Online]. Available: https://www.hindawi.com/journals/ijap/2018/2094637/

[37] M. E. Halpern and D. C. Ng, “Optimal tuning of inductive wireless power links: Limits of performance,” vol. 62, no. 3, pp. 725–732. doi: 10.1109/TCSI.2014.2386771. [Online]. Available: http://ieeexplore.ieee.org/document/7024943/

[38] X. Qu, H. Han, S.-C. Wong, C. K. Tse, and W. Chen, “Hybrid IPT topologies with constant current or constant voltage output for battery charging applications,” vol. 30, no. 11, pp. 6329–6337. doi: 10.1109/TPEL.2015.2396471. [Online]. Available: http://ieeexplore.ieee.org/document/7018969/

[39] A. N. Azad, A. Echols, V. A. Kulyukin, R. Zane, and Z. Pantic, “Analysis, optimization, and demonstration of a vehicular detection system intended for dynamic wireless charging applications,” vol. 5, no. 1, pp. 147–161. doi: 10.1109/TTE.2018.2870339. [Online]. Available: https://ieeexplore.ieee.org/document/8466857/

[40] X. Dai, X. Li, Y. Li, and A. P. Hu, “Maximum efficiency tracking for wireless power transfer systems with dynamic

coupling coefficient estimation," vol. 33, no. 6, pp. 5005–5015. doi: 10.1109/TPEL.2017.2729083. [Online]. Available: https://ieeexplore.ieee.org/document/7984817/

[41] D. Kobayashi, T. Imura, and Y. Hori, "Real-time coupling coefficient estimation and maximum efficiency control on dynamic wireless power transfer for electric vehicles," in *2015 IEEE PELS Workshop on Emerging Technologies: Wireless Power (2015 WoW)*. IEEE. doi: 10.1109/WoW.2015.7132799. ISBN 978-1-4799-6610-3 pp. 1–6. [Online]. Available: http://ieeexplore.ieee.org/document/7132799/

[42] Z.-H. Wang, Y.-P. Li, Y. Sun, C.-S. Tang, and X. Lv, "Load detection model of voltage-fed inductive power transfer system," vol. 28, no. 11, pp. 5233–5243. doi: 10.1109/TPEL.2013.2243756. [Online]. Available: http://ieeexplore.ieee.org/document/6425491/

[43] S. Hu, Z. Liang, Y. Wang, J. Zhou, and X. He, "Principle and application of the contactless load detection based on the amplitude decay rate in a transient process," vol. 32, no. 11, pp. 8936–8944. doi: 10.1109/TPEL.2017.2656253. [Online]. Available: http://ieeexplore.ieee.org/document/7829319/

[44] Y.-G. Su, H.-Y. Zhang, Z.-H. Wang, A. Patrick Hu, L. Chen, and Y. Sun, "Steady-state load identification method of inductive power transfer system based on switching capacitors," vol. 30, no. 11, pp. 6349–6355. doi: 10.1109/TPEL.2015.2411755. [Online]. Available: http://ieeexplore.ieee.org/document/7058385/

[45] Wireless charging market size | industry report, 2022. [Online]. Available: https://www.grandviewresearch.com/industry-analysis/wireless-charging-market

[46] Automated guided vehicle market: Laser guidance technology to gain momentum: Global industry analysis and opportunity assessment, 2019 - 2029. [Online]. Available: https://www.futuremarketinsights.com/reports/automated-guided-vehicles-market

[47] Emerging trends, drivers and challenges in the electric wheelchairs market 2019-2023 | technavio. [Online]. Available: https://www.businesswire.com/news/home/20190821005509/en/Emerging-Trends-Drivers-Challenges-Electric-Wheelchairs-Market

[48] S. Debnath, A. Banerjee, and V. Namboodiri, "Adapting RANSAC SVM to detect outliers for robust classification," in *Procedings of the British Machine Vision Conference 2015*. British Machine Vision Association. doi: 10.5244/C.29.168. ISBN 978-1-901725-53-7 pp. 168.1–168.11. [Online]. Available: http://www.bmva.org/bmvc/2015/papers/paper168/index.html

Appendix A:

Appendix A.1: Full bridge inverter

Referring Figure 3.3, during interval t_0-t_1, switches S_1 and S_4 are on and S_3 and S_2 are off. During this interval, V_{in} is applied positively to the primary side. This is power transfer interval where primary current flows through S_1, transformer primary, resonant inductor (L_s) and S_4. During this mode power flows to the output through rectifier diodes D_3 and D_4 and also energy stored in L_s. During the interval t_1-t_2, the energy stored in L_rx is transferred to the output. In this interval, S_4 is turned off, the freewheel current caused by the leakage inductance of L_s continues to flow through body diode of S_3 during this transition period. This freewheeling current charge the parasitic capacitor of switch S_4 where discharge the parasitic capacitor of S_3. The parasitic capacitor of S_4 is charged until it reached charge equal to V_{in} and parasitic capacitor of S_3 is discharged until the voltage between drain and source of S_3 reaches zero. Energy accumulated in L_s remains even after charging/discharging the parasitic capacitors. Since voltage at the both ends of the transformer is almost zero so no power is transfer during this interval.

During the interval t_2-t_3, switch S_3 is turned on and the body diode of S_3 is still turned on so the voltage between the drain and source is zero. The freewheeling current continues to flow in the primary and the secondary side of the circuit. In the interval of t_3-t_4, S_1 is turned off and parasitic capacitance of S_1 is charged where parasitic capacitance of S_2 is discharged. The freewheel current continues to flow in the both side of the circuit. When charging/discharging of the parasitic capacitors completed, the freewheel current still flows through body diode of S_2 as energy is accumulating in L_s. The voltage between drain and source of S_2 is kept zero while current is flowing through the body diode of S_2. In t_4-t_5, S_2 is turned on, at this moment the voltage between the drain and source is zero. During the transition of off to on the freewheeling current of L_s also continue to flow. The power is transferred from primary to secondary side. During t_5-t_6, S_3 is turned off, the energy accumulated in L_s generates freewheel current to charge parasitic capacitor of S_3 and discharge parasitic capacitor of S_4. After the charging/discharging, the current flow through body diode of S_4 at this phase. In t_6-t_7, S_4 is turned on and since the body diode of S_2 is turned on, the voltage between drain and source is zero. The freewheel current continues to flow. During t_7-t_8, S_2 is turned off, the parasitic capacitance of S_2 is charged and parasitic capacitance of S_1 is discharged

through the freewheeling current of L_{s}. After the charging/discharging of parasitic capacitors the freewheeling current flows through the body diode of S_1. At this moment the voltage across drain and source of S_1 is almost zero which will turn of in the next cycle.